Intrinsic activity development unfolds along a sensorimotor–association cortical axis in youth

Valerie J. Sydnor[1,2], Bart Larsen[1,2], Jakob Seidlitz [2,3,4], Azeez Adebimpe[1,2], Aaron F. Alexander-Bloch [2,3,4], Dani S. Bassett [2,5,6,7,8,9], Maxwell A. Bertolero [1,2], Matthew Cieslak [1,2], Sydney Covitz[1,2], Yong Fan [10,11], Raquel E. Gur[2,3,4], Ruben C. Gur[2,4], Allyson P. Mackey[12], Tyler M. Moore [2,4], David R. Roalf [2], Russell T. Shinohara[11,13,14] & Theodore D. Satterthwaite [1,2,4,11,13] ✉

Animal studies of neurodevelopment have shown that recordings of intrinsic cortical activity evolve from synchronized and high amplitude to sparse and low amplitude as plasticity declines and the cortex matures. Leveraging resting-state functional MRI (fMRI) data from 1,033 youths (ages 8–23 years), we find that this stereotyped refinement of intrinsic activity occurs during human development and provides evidence for a cortical gradient of neurodevelopmental change. Declines in the amplitude of intrinsic fMRI activity were initiated heterochronously across regions and were coupled to the maturation of intracortical myelin, a developmental plasticity regulator. Spatiotemporal variability in regional developmental trajectories was organized along a hierarchical, sensorimotor–association cortical axis from ages 8 to 18. The sensorimotor–association axis furthermore captured variation in associations between youths' neighborhood environments and intrinsic fMRI activity; associations suggest that the effects of environmental disadvantage on the maturing brain diverge most across this axis during midadolescence. These results uncover a hierarchical neurodevelopmental axis and offer insight into the progression of cortical plasticity in humans.

Elucidating how developmental plasticity spatially and temporally progresses across the human cortex has implications for understanding healthy brain development and windows of developmental vulnerability and opportunity[1–3]. In particular, demarcating regionally specific periods of enhanced and diminished malleability can provide insight into which cortical regions will be maximally impacted by insults and interventions at distinct developmental stages. Prior studies have therefore aimed to uncover the spatiotemporal evolution of neurodevelopmental change across the cortical mantle. Such studies have consistently shown that postnatal neurodevelopment is heterochronous, with sensory and motor cortices maturing earlier than association cortices[4]; this temporal trend has been shown for cortical volume[5,6], connectivity[7], myelination[8,9] and cellular properties[10,11]. However, beyond this coarse division, there is marked spatiotemporal developmental variability that remains undercharacterized. We recently proposed a unifying framework that contextualizes asynchronous maturation between sensorimotor and association cortices as two ends of a continuous axis of neurodevelopmental plasticity[4]. This framework

posits that during childhood and adolescence, developmental plasticity progresses along the sensorimotor–association (S–A) cortical axis: a dominant, hierarchical axis of human brain organization along which diverse neurobiological properties are patterned[4,12–15].

In the present study, we aimed to empirically evaluate our hypothesis that plasticity unfolds along the S–A axis by studying the developmental refinement of intrinsic (that is, spontaneous or non-evoked) activity, a putative functional marker of local plasticity described in animal models. Studies of the developing murine sensory cortex have provided evidence that a potentiation of high-amplitude, synchronized intrinsic activity characterizes earlier stages of development with heightened plasticity[16–18]. As plasticity declines and the cortex matures, intrinsic activity evolves from prevalent and globally synchronized to suppressed and sparse, becoming more heterogeneously distributed in space and time in the adult cortex[18–21]. This stereotyped refinement of intrinsic activity has been linked to maturational increases in inhibitory neurotransmission and intracortical myelination, two plasticity-regulating processes that refine cortical circuit dynamics[17,22–25]. Accordingly, this stereotyped refinement of intrinsic activity provides an ongoing readout of local circuit plasticity, with more correlated, high-amplitude spontaneous neural recordings serving as a functional hallmark of still-malleable cortices[16,17,26,27]. Importantly, intrinsic cortical activity can be studied non-invasively with resting-state functional MRI (fMRI), which provides an opportunity to characterize the spatiotemporal maturation of a potential plasticity signature in the human brain.

Simultaneous fMRI with electrophysiology or calcium imaging has demonstrated how low-frequency fluctuations in the resting fMRI blood oxygen level-dependent (BOLD) signal are coupled with changes in intrinsic neural activity patterns[28–31]. A greater level of intrinsic activity and more synchronized activity—activity characteristic of immature, plastic cortices—can increase the amplitude of low-frequency BOLD fluctuations. It has therefore been hypothesized that the amplitude of low-frequency fluctuations[32], or BOLD 'fluctuation amplitude', will be higher when cortical plasticity is enhanced[26,33]. Indeed, experimentally manipulating biological regulators of developmental plasticity has been shown to elicit changes in local BOLD fluctuations[34]. Moreover, in a recent landmark study of human brain plasticity, deprivation-induced somatomotor cortex plasticity produced local increases in BOLD fluctuation amplitude[35].

Here, we harness BOLD fluctuation amplitude to index spatially localized, age-dependent changes in intrinsic activity and test the overarching framework that developmental programs cascade hierarchically along the cortex's S–A axis during youth. We expected that the development of fluctuation amplitude would be primarily characterized by heterochronous declines along the S–A axis. Moreover, we predicted that declines in fluctuation amplitude would be influenced by the maturation of intracortical myelin, which constrains plasticity in developing neural circuits and refines spontaneous firing[25]. Last, we hypothesized that youths' developmental environments would impact the maturation of this measure. Instrumental work in animal models has shown that enriched (versus deprived) developmental environments affect the maturation of plasticity-regulating mechanisms, including intracortical myelin[36], inhibitory interneurons[37] and perineural nets[38], typically in a manner that facilitates continued plasticity[39]. Data from human studies have additionally shown that individuals raised in more socioeconomically disadvantaged environments exhibit characteristics that could reflect a faster pace of biological and brain development[39–41]. Cross-species findings thus indicate that environmental deprivation may accelerate cortical development and prematurely limit plasticity. We explore this possibility by studying whether greater environmental disadvantage is associated with functional markers suggestive of lower cortical plasticity during youth. As described below, our in vivo analysis of a signature of neurodevelopmental plasticity illuminated by animal models reveals that the S–A axis captures not only the hierarchical layout of diverse cortical properties but also the temporal unfolding of developmental change and effects of the developmental environment.

Results

We studied how intrinsic activity is refined across the developing cortex in a cross-sectional sample of 1,033 youths aged 8–23 years old. Fluctuation amplitude, computed as the average power of low-frequency (0.01–0.08 Hz) fluctuations in the time-varying fMRI signal, was used to index the overall level and coherence of intrinsic cortical activity. Greater and more synchronized neural activity increases the power of neural recordings and has been shown to increase the amplitude of BOLD fluctuations[29–31]. To characterize maturational changes in BOLD fluctuation amplitude in individual cortical regions, we fit region-specific generalized additive models (GAMs) with a smooth term for age; sex and in-scanner head motion were included as linear covariates. Each GAM estimates a smooth function (the model age fit) that describes the relationship between fluctuation amplitude and age, thereby modeling a region's developmental trajectory. The first derivative of this smooth function represents the rate of change in fluctuation amplitude at a given developmental timepoint. We tested whether GAM-derived developmental effects provide support for a hierarchical neurodevelopmental framework. We also confirmed that developmental effects were robust to controls for in-scanner motion, medication use, vascular effects, T2* signal strength, global BOLD properties and cortical atlas.

Development of intrinsic fMRI activity varies across the cortex

Fluctuation amplitude significantly changed with age in the developmental window studied in nearly all cortical regions (false discovery rate-adjusted P value (P_{FDR}) < 0.05 in 95% of regions). To provide insight into the overall magnitude and direction of regional age effects, we calculated the variance explained by age (partial R^2; the effect magnitude) and the sign of the average derivative of the age fit (the effect direction). The magnitude and direction of age effects differed across the cortex (Fig. 1a), signifying that there is variability in the maturation of intrinsic activity across the developing cortex. Indeed, by visualizing age fits across regions, we observed a cortical continuum of developmental trajectories ranging from large and prolonged decreases to inverted U-shaped curves (Fig. 1b). Nearly all sensory regions showed continuous declines in fluctuation amplitude from early childhood to adolescence, as illustrated by the model fit for area V1 (Fig. 1c), which significantly decreased until the age of 18 years. This age fit is consistent with a progressive reduction, sparsification or decorrelation of non-evoked cortical activity with age. By contrast, in select cortical regions such as the midcingulate gyrus (Fig. 1c), fluctuation amplitude only began to decline in later childhood or early adolescence. Finally, many regions in transmodal association cortex (for example, the dorsolateral prefrontal cortex; Fig. 1c) displayed significant increases in fluctuation amplitude until early to midadolescence, typically followed by amplitude decreases. This inverted U-shaped trajectory suggests that there is heightened, synchronized activity in transmodal cortices at the start of adolescence.

We examined whether regional age fits differed by sex or could be accounted for by differences in participant pubertal stage. We first tested for age-by-sex interactions in each cortical region and found no significant effects (P_{FDR} > 0.05 for all interactions), indicating that the timing of developmental change did not significantly differ between males and females in this age range. Next, we explored the potential impact of puberty by including participant pubertal stage (prepubertal, midpubertal or postpubertal) as a factor in regional GAMs. While the linear effects of pubertal stage on fluctuation amplitude tended to cohere with the observed age effects (positive effects in frontal transmodal regions and negative effects in posterior unimodal regions), pubertal stage did not explain significant variance in fluctuation amplitude above and beyond age in any cortical region (P_{FDR} > 0.05 for all
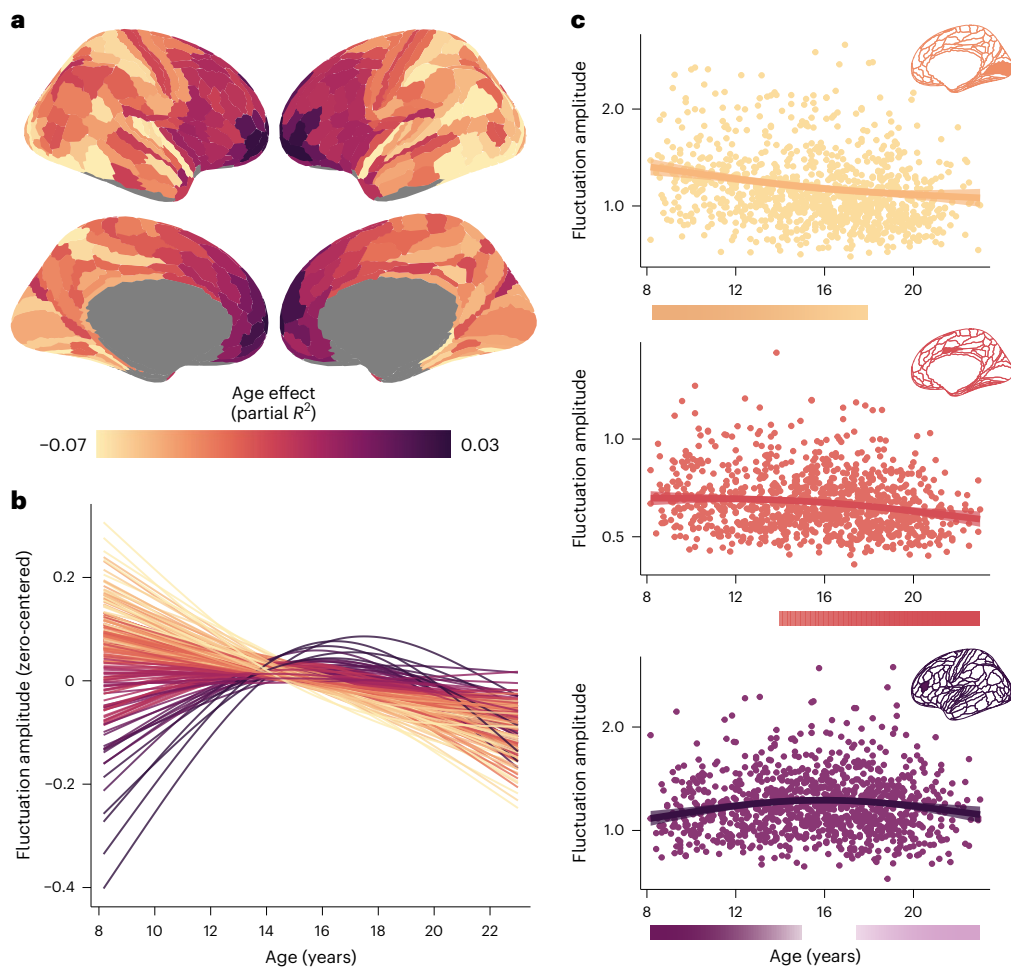
Fig. 1 | Developmental refinement of fluctuation amplitude varies across the cortex. a, The heterogeneous patterning of fluctuation amplitude age effects (partial R^2) is displayed across the cortical surface. **b**, Fluctuation amplitude developmental trajectories (zero-centered GAM smooth functions) are shown for all left hemisphere cortical regions, revealing a spectrum of age-related change. Trajectories are colored by each region's age effect using the color bar in **a**. **c**, Fluctuation amplitude developmental trajectories are shown overlaid on data from all participants for the primary visual cortex (area V1; top, yellow), the midcingulate gyrus (area p24pr; middle, pink) and the dorsolateral prefrontal cortex (area IFSa; bottom, purple). Regional trajectories represent the GAM-predicted fluctuation amplitude value at each age with a 95% credible interval band. The color bars below each regional plot depict the age window(s) wherein fluctuation amplitude significantly changed in that region, shaded by the rate of change, as determined by the first derivative of the age function. Windows of significant age-related change are developmental periods wherein the simultaneous 95% confidence interval for the first derivative did not include 0 (two sided).

pubertal stage effects). Moreover, accounting for pubertal stage did not alter regional age fits or age effects; age effects were highly correlated when age was modeled alone and when both age and pubertal stage were modeled together ($r = 0.89$). These findings suggest that age-dependent changes in intrinsic fMRI activity amplitude are heterogeneous across the cortex, are present across sexes and are not driven by pubertal stage. More broadly, the present results establish that maturational trajectories diverge between sensory and association cortices.

Development of intrinsic fMRI activity mirrors myelin maturation

Prior work in animal models has shown that as the cortex transitions from plastic to mature, intrinsic cortical activity develops from prevalent and synchronized, producing high-amplitude neural recordings, to sparse and decorrelated, producing lower-amplitude recordings. These observations suggest that age-dependent changes in the amplitude of BOLD fluctuations could, in part, reflect changes in cortical plasticity[26,35]. We therefore endeavored to understand whether the development of fluctuation amplitude is related to the maturation of intracortical myelin, a key regulator and restrictor of cortical plasticity.

We leveraged the recent work of Baum et al.[42] who studied the development of the T1-weighted/T2-weighted (T1w/T2w) ratio, a structural MRI measure sensitive to cortical myelin content, in an independent sample of youths ($n = 628$; 8–21 years old). These authors quantified the magnitude of age-related myelination (the partial R^2 of the T1w/T2w ratio age effect) and demarcated the age of maximal myelin growth (the age with a maximal rate of T1w/T2w ratio increase) within individual cortical regions. In comparing T1w/T2w ratio and fluctuation amplitude neurodevelopmental features, we unveiled substantial spatial and temporal correspondence between the refinement of these measures with age. Age-related changes (indexed by the signed partial R^2) in these two putative plasticity-sensitive measures were strongly inversely correlated across cortical regions ($r = -0.67$, spin test P value (P_{spin}) = 0.00045), with regions showing larger increases in myelin content from childhood to early adulthood also undergoing larger decreases in BOLD signal amplitude (Fig. 2a,b). This finding accords with ample evidence of causal, bidirectional relationships between changes in neural activity patterns and changes in myelination[43,44] and suggests a possible mechanistic link between microstructural refinement and changes in circuit activity during brain development.
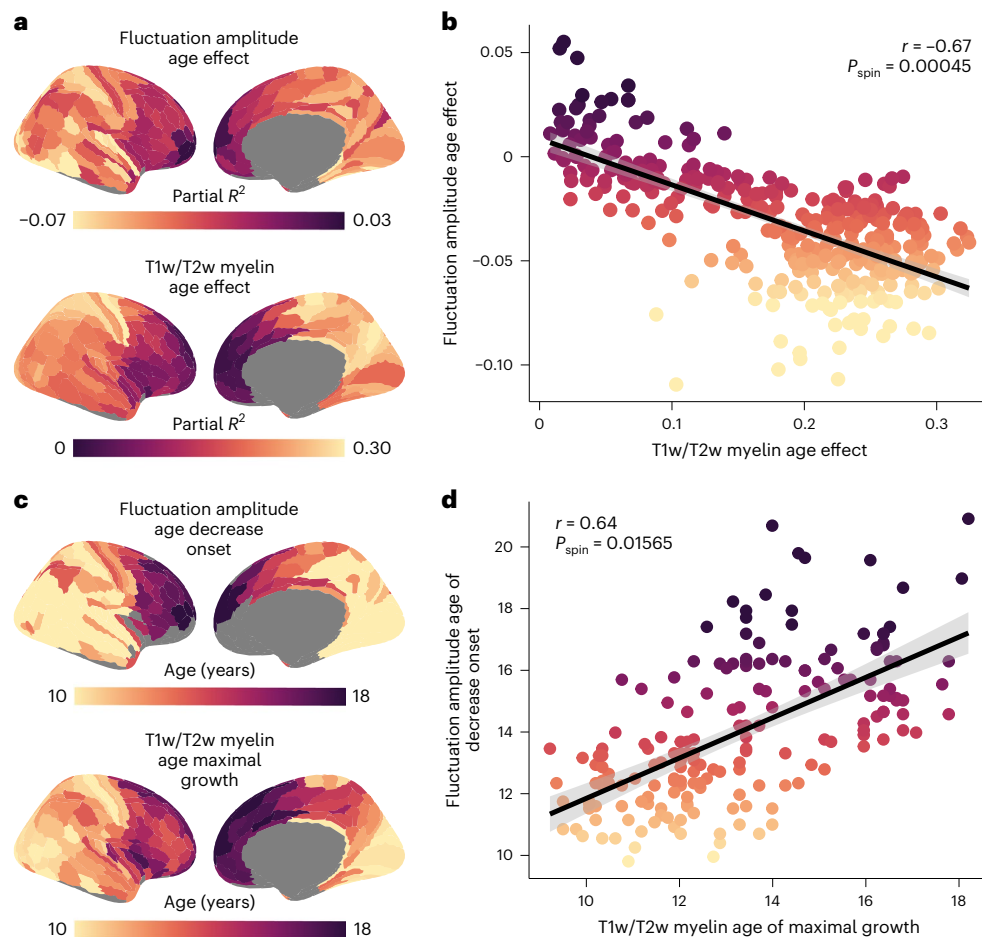
Fig. 2 | Development of fluctuation amplitude spatially and temporally parallels cortical T1w/T2w ratio development. a, The cortical distribution of fluctuation amplitude age effects closely resembles the distribution of T1w/T2w ratio age effects, suggesting interdependent refinement of cortical function and microstructure in youth. Age effects (partial R^2) are signed by the sign of the average first derivative of the age smooth function. **b**, Regions that show larger declines in fluctuation amplitude during childhood and adolescence additionally exhibit greater increases in the cortical T1w/T2w ratio in this developmental period. A Spearman's correlation between age effects for these two measures was significant ($r = -0.67$, $P_{spin} = 0.00045$) as assessed by a conservative spin-based spatial rotation test. The negative linear fit between these measures is shown with a 95% confidence interval. **c**, Maps depicting the age at which

fluctuation amplitude began to decrease (earliest significant negative derivative of the age function) and the age of maximal T1w/T2w-indexed myelin growth (largest significant derivative of the age function) reveal temporal similarity in the development of these two measures in youth. **d**, Across regions, the age at which fluctuation amplitude began to significantly decrease is closely coupled to the age at which the T1w/T2w ratio shows a maximal rate of increase, providing evidence for temporal coordination between functional and structural maturation. A Spearman's correlation between these temporal measures was significant ($r = 0.64$, $P_{spin} = 0.01565$) as assessed by the spatial rotation test procedure. The positive linear relationship between these two measures is plotted with a 95% confidence interval.

To further study this link, we investigated whether there was a temporal relationship between increases in the T1w/T2w ratio and decreases in fluctuation amplitude. We first quantified the age at which fluctuation amplitude began to significantly decrease in each region and found that initial decreases in fluctuation amplitude were staggered heterochronously across the cortex, with select medial prefrontal and frontopolar regions showing no period of significant decline. Nearly half of regions (46%) showed a significant decrease in fluctuation amplitude at age 8, implying that BOLD amplitude in these regions likely begins to decline before the youngest age studied in this dataset. Across the rest of the cortex, however, fluctuation amplitude began to decline later in youth; in these cortices, a greater delay in the onset of fluctuation amplitude decline was associated with a later peak rate of T1w/T2w-indexed cortical myelin growth ($r = 0.64$, $P_{spin} = 0.01565$; Fig. 2c,d). Notably, ages of fluctuation amplitude decrease onset and maximal T1w/T2w increase were not simply correlated but also showed a minimal temporal offset in years, indicating that they were closely coupled in time (average offset of 0.7 years; see also the best fit

line for Fig. 2d). Taken together, these results appear to link later-onset reductions in the amplitude of spontaneous fMRI activity to delayed maturation of a main regulator of developmental plasticity.

Developmental variability is patterned along the S–A axis
A primary goal of this work was to systematically assess whether the sequence of neurodevelopmental change progresses hierarchically across the cortical mantle. Having observed that fluctuation amplitude development tightly paralleled development of a structural plasticity regulator and broadly diverged between sensorimotor and association cortices, we next sought to determine whether developmental patterns spatially conformed to the S–A axis[4]. The S–A axis is a prominent axis of cortical organization that is rank ordered from primary cortices supporting sensation and movement (lowest ranks), to multimodal cortices supporting multisensory integration and attention (middle ranks), to transmodal cortices supporting cognitive control and socioemotional functioning (highest ranks). This axis captures concerted variability in the layout of heterogeneous structural, metabolic, cellular, molecular, transcriptomic

and electrophysiological properties across the cortex[4,12–15,45]. Moreover, the S–A axis is spatially coupled to the brain's anatomical[45], functional[14] and evolutionary[46] hierarchies; thus, each cortical region's rank in the axis reflects its relative position in a global cortical hierarchy.

We first examined whether interregional differences in the development of fluctuation amplitude reflected interregional differences in S–A axis rank. Age effects and S–A axis ranks were correlated across regions ($r = 0.54$, $P_{spin} = 0.00215$), with large negative age effects characterizing the S–A axis's sensorimotor pole and smaller positive age effects distinguishing its association pole. We additionally observed continuous variation in the age at which fluctuation amplitude began to significantly decrease along this organizational axis. When considering regions that showed an initial onset of decline within the age range studied as above, we found that fluctuation amplitude began to decline at a progressively later age in regions ranked higher in the S–A axis ($r = 0.68$, $P_{spin} = 0.00110$). Hence, cortices at the top of the cortical hierarchy exhibit the smallest and latest-onset declines in the amplitude of intrinsic fMRI fluctuations during childhood and adolescence.

Following this initial analysis, we further probed the extent to which maturational trajectories differed as a function of S–A axis rank by mapping the principal spatial axis of fluctuation amplitude development. To accomplish this mapping, we performed a principal-component analysis (PCA) on the age fits estimated by regional GAMs (Fig. 1b); this approach considers the entire fluctuation amplitude developmental trajectory rather than only one property of the age fit (for example, the age at which it starts to decline). The first PC from this PCA explained 87% of the variance in developmental profiles and can therefore be conceptualized as the principal axis of intrinsic fMRI activity development. This principal developmental axis closely resembled the S–A axis (Fig. 3a). Accordingly, regional loadings onto the principal developmental axis were very highly correlated with regional S–A axis ranks ($r = 0.70$, $P_{spin} < 0.0001$; Fig. 3b), demonstrating that a substantial degree of spatiotemporal variance in developmental profiles was explained by the S–A axis.

The PCA of developmental fits suggests that the spatial and temporal maturation of intrinsic cortical activity conforms to the hierarchical organization of the cortex. In support of this conclusion, we confirmed that principal developmental axis loadings additionally correlated with anatomical[45] ($r = -0.61$), functional[14] ($r = 0.60$) and evolutionary[46] ($r = 0.32$) cortical hierarchies. However, the principal developmental axis was significantly more correlated with the S–A axis

than with these three hierarchies, which were defined using unimodal data ($P < 0.001$ for all three statistical tests comparing the magnitude of two dependent, overlapping corrections). Neurodevelopmental trajectories were therefore more parsimoniously captured by the S–A axis, which combines information from all three cortical hierarchies and multiple additional data types. To directly illustrate the manner in which developmental trajectories for fluctuation amplitude evolve from the sensorimotor to the association end of the S–A axis, we divided the axis into 10 decile bins and averaged age fits across all regions in a bin. The continuous spectrum of developmental trajectories visible at the regional level (Fig. 1b) was recapitulated by S–A axis deciles (Fig. 3c).

Development is hierarchical through adolescence

The above results underscore that between the ages of 8 and 23 years, age-related changes in fMRI-indexed intrinsic activity amplitude are patterned along the brain's S–A axis. We next aimed to elucidate whether
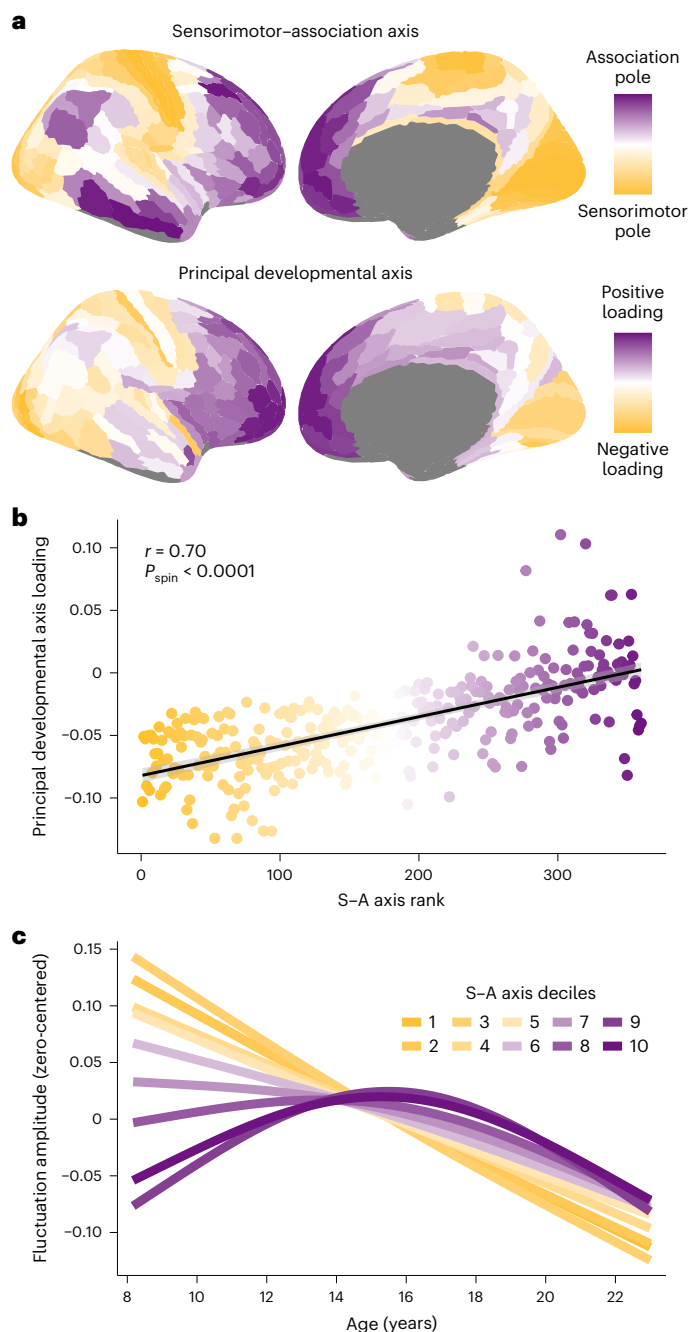
Fig. 3 | The principal axis of fluctuation amplitude development exhibits convergent spatial embedding with the S–A axis. a, The principal axis of fluctuation amplitude development closely resembles the S–A axis, illustrating that the spatiotemporal maturation of intrinsic fMRI activity amplitude aligns to the brain's global cortical hierarchy. The S–A axis, derived in Sydnor et al.[4], is a dominant axis of cortical feature organization that spans continuously from primary and unimodal sensory and motor cortices (sensorimotor pole; dark yellow) to transmodal heteromodal and paralimbic association cortices (association pole; dark purple). The principal developmental axis is the first component from a PCA conducted on regional fluctuation amplitude maturational trajectories. This component quantitatively captures cortex-wide differences in maturational patterns along a unidimensional spatial gradient. **b**, Across the cortex, principal developmental axis loadings are strongly related to S–A axis ranks (linear association shown with a 95% confidence interval). The Spearman's correlation between these two measures, which represent developmental and organizational maps, was significant ($r = 0.70$, $P_{spin} < 0.0001$), as assessed by a conservative spin-based spatial rotation test. **c**, Average model fits depicting the relationship between fluctuation amplitude and age are shown for deciles of the S–A axis. To generate average decile fits, the S–A axis was divided into 10 bins each consisting of 33 or 34 regions, and age smooth functions were averaged across all regions in a bin. The first decile (darkest yellow; linear decline) represents the sensorimotor pole of the axis, and the tenth decile (darkest purple; inverted U) represents the association pole of the axis. Maturational trajectories diverged most between S–A axis poles and varied continuously between them.
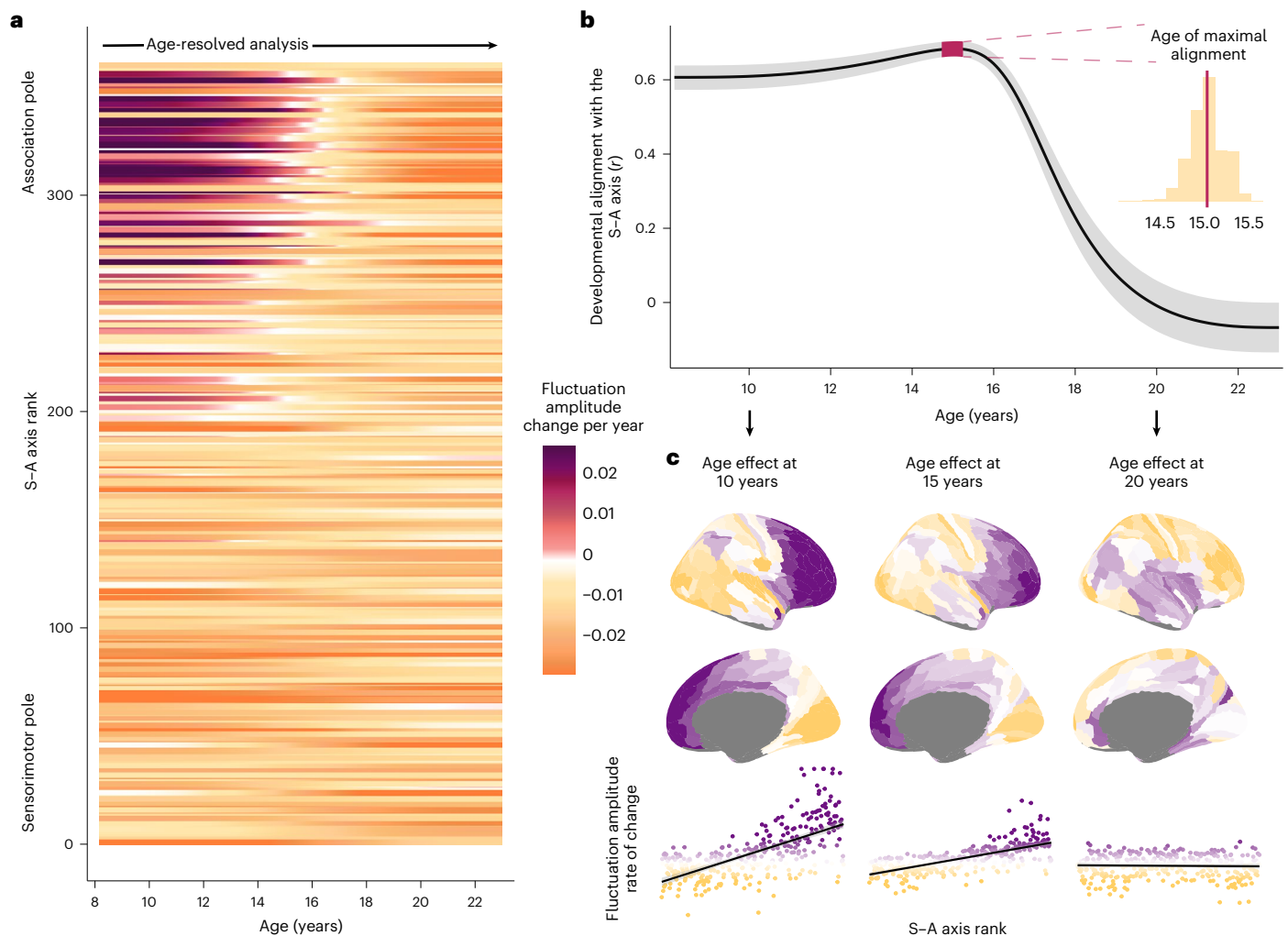
Fig. 4 | Neurodevelopment unfolds along the S–A axis until late adolescence.
a, The rate and direction of developmental change in fluctuation amplitude is displayed for each cortical region from ages 8 to 23 years. Regions are ordered along the *y* axis by S–A axis rank. Fluctuation amplitude rate of change, expressed as the change in amplitude per year, was estimated from the first derivative of each region's GAM smooth function for age. Cortical regions near the association pole of the S–A axis exhibit unique increases in fluctuation amplitude through childhood that culminate in adolescent BOLD amplitude peaks.
b, Developmental change in intrinsic fMRI activity amplitude aligns with the S–A axis from childhood until late adolescence. The line plot displays age-specific correlation values (*r*) between regional rates of fluctuation amplitude change and regional S–A axis ranks from ages 8 to 23 years. To obtain reliable estimates of this correlation value at each age, we sampled 10,000 draws from the posterior derivative of each region's age smooth function and quantified age-specific correlations between derivatives and S–A axis ranks for each draw. The median

correlation value obtained across all draws is depicted by the black line, and the 95% credible interval around this value is represented by the gray band. We additionally determined the age of maximal alignment between fluctuation amplitude change and S–A axis rank for all 10,000 draws. The 95% credible interval for the age of maximal alignment is depicted on the line plot by the pink band. The full distribution of ages obtained from all draws is portrayed in the inset histogram. **c**, Age-specific developmental effects (first derivative maps) are visualized on the cortical surface at ages 10, 15 and 20 years. Maps are shown above scatter plots that depict the linear relationship (with a 95% confidence interval band) between regional S–A axis ranks and regional age-specific rates of fluctuation amplitude change. Scatter plot points are colored by age-specific rates of change. Developmental refinement of fluctuation amplitude is governed by the S–A axis at ages 10 and 15 years. By age 20, further refinement of fluctuation amplitude is unrelated to the S–A axis.

this neurodevelopmental pattern was most pronounced during a specific age range or if it was equally present across all ages studied. To explore these possibilities, we first calculated each cortical region's rate of change in fluctuation amplitude at 1-month intervals between ages 8 and 23 years. Notably, visualizing regional rates of change across the S–A axis (Fig. 4a) confirmed that preadolescent increases in fluctuation amplitude were uniquely confined to higher-order association cortices. Using these data, we next performed an age-resolved analysis, where at each 1-month interval, we calculated the correlation between regional rates of amplitude change and regional S–A axis ranks. This procedure generates age-specific correlation values that quantify the extent to which maturational change is spatially ordered along the hierarchy of

the S–A axis at a given developmental timepoint. This analysis confirmed a robust correlation between developmental change and S–A axis rank from age 8 to 17 years (Fig. 4b,c). A maximal correlation value of *r* = 0.68 (95% credible interval of 0.66 to 0.70) was observed at age 15.0 years (95% credible interval of 14.7 to 15.3 years), indicating peak alignment between neurodevelopment and the S–A axis in midadolescence. However, following this peak, the correlation between regional developmental effects and S–A axis position rapidly declined, dropping to 0 by age 19.3 years (95% credible interval of 18.7 to 20.2 years). These findings suggest that the brain's developmental program is hierarchical through late adolescence. Following adolescence, however, there may be a programmed switch in the spatial organization of subsequent age-related change.
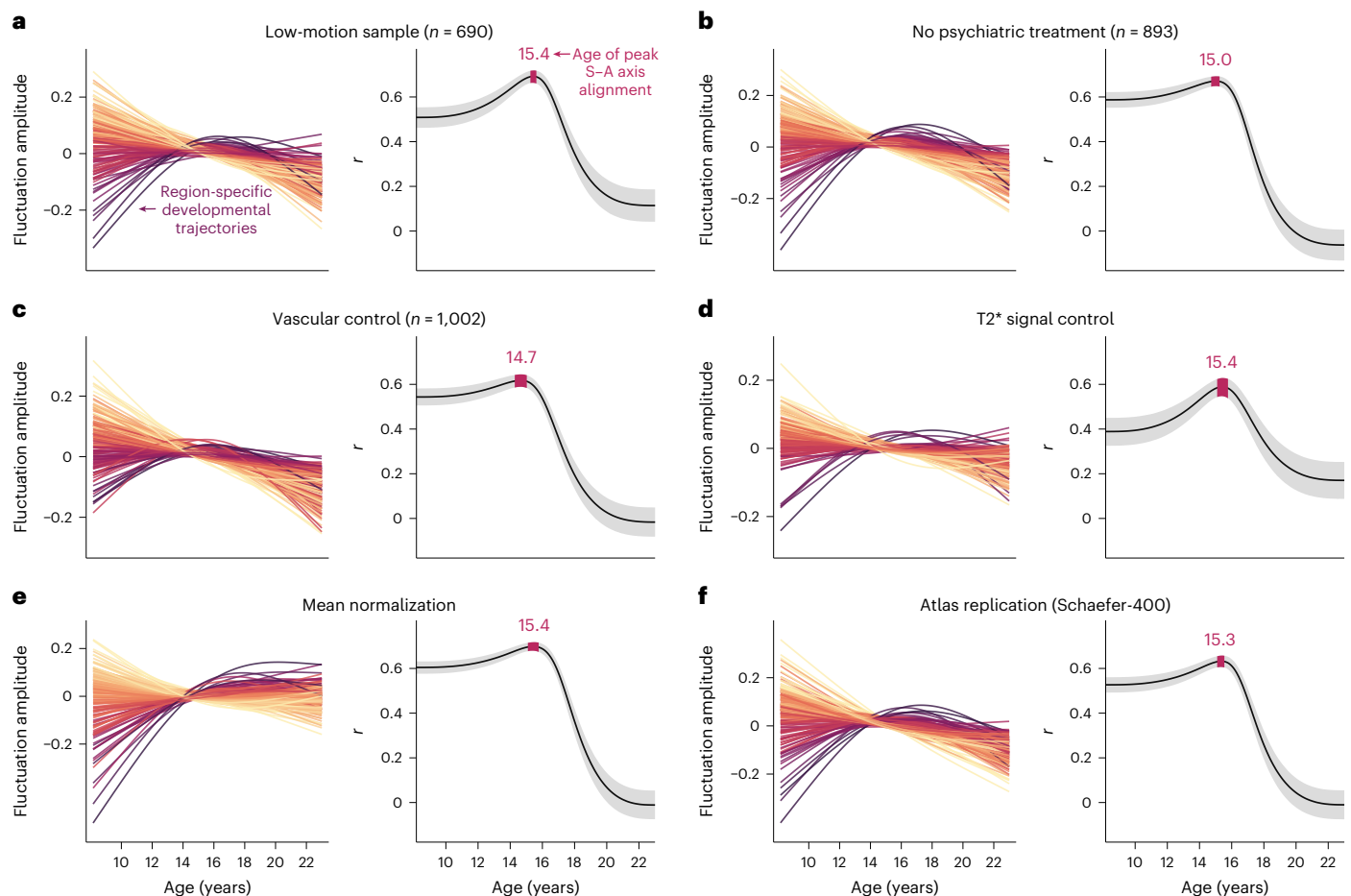
Fig. 5 | Region-specific and cortex-wide developmental patterns are robust to methodological variation. a–f, Key results are shown for each of the six sensitivity analyses performed. For each analysis, the left plot shows fluctuation amplitude developmental trajectories (zero-centered GAM smooth functions) for left hemisphere regions colored by age effects. The right plot presents the age-resolved analysis of the correlation between developmental change in fluctuation amplitude and S–A axis rank from ages 8 to 23 years. Both the medial correlation value (r) and the 95% credible interval around this value are shown for the age-resolved analysis. All six sensitivity analyses yielded convergent region-specific and cortex-wide results, confirming that our developmental findings were not being driven by head motion in the scanner (**a**), the use of psychotropic medications (**b**), age-related changes in cerebrovascular perfusion (**c**), interscan differences in T2* signal strength (**d**), global effects (**e**) or the specific atlas used for cortical parcellation (**f**).

## Development results are robust to methodological variation

To ensure that the developmental effects observed were robust to methodological variation and potential confounds, we performed six sensitivity analyses. We evaluated if age-dependent changes in regional fluctuation amplitude were driven by in-scanner head motion, medication use, local cerebral blood flow, regional mean signal intensity, global amplitude differences or the choice of cortical atlas. In the first two sensitivity analyses, regional GAMs were rerun in two-thirds of the sample with the lowest in-scanner head motion (n = 690; Fig. 5a) and in a sample that excluded individuals with current psychoactive medication use or a history of psychiatric hospitalization (n = 893; Fig. 5b). In the next two sensitivity analyses, regional GAMs were refit while additionally controlling for regional cerebral blood flow estimated from arterial spin labeling (ASL) data (n = 1,002; Fig. 5c) or regional mean T2* signal intensity (Fig. 5d). In the final two sensitivity analyses, regional GAMs were refit with whole-brain mean-normalized fluctuation amplitude (Fig. 5e) or fluctuation amplitude averaged within Schaefer-400 atlas regions (Fig. 5f) as the dependent variables.

In each of the six sensitivity analyses, region-specific fluctuation amplitude maturational trajectories closely mirrored the developmental fits from the main analysis, with negative age effects observed in most cortices but positive effects seen in select transmodal association

cortices. Consequently, regardless of the sample used or controls performed, a cortical region's age effect was fundamentally and significantly (all P_{spin} < 0.05) related to its position in the S–A axis (main analysis: r = 0.54; low-motion sample: r = 0.56; no psychiatric treatment: r = 0.51; vascular control: r = 0.51; T2* signal control: r = 0.49; mean normalization: r = 0.66; atlas replication: r = 0.43). Furthermore, for all sensitivity analyses, the age-resolved analysis confirmed a strong correlation between the rate of fluctuation amplitude change and S–A axis rank from childhood to late adolescence, with the peak age of neurodevelopmental alignment to this axis occurring during adolescence. These analyses verify that findings concerning the nature and patterning of age-dependent changes in spontaneous cortical fMRI activity are robust to methodological variation.

Environmental effects vary along the S–A axis in adolescence

During brain maturation, environmental inputs can interact with neurodevelopmental malleability to become cortically embedded, suggesting that variability in children's environments may be reflected in individual differences in development-linked brain changes. We therefore explored whether interindividual differences in cortical intrinsic fMRI activity may be partly explained by variability in youths' neighborhood environments. Multivariate features of each child's
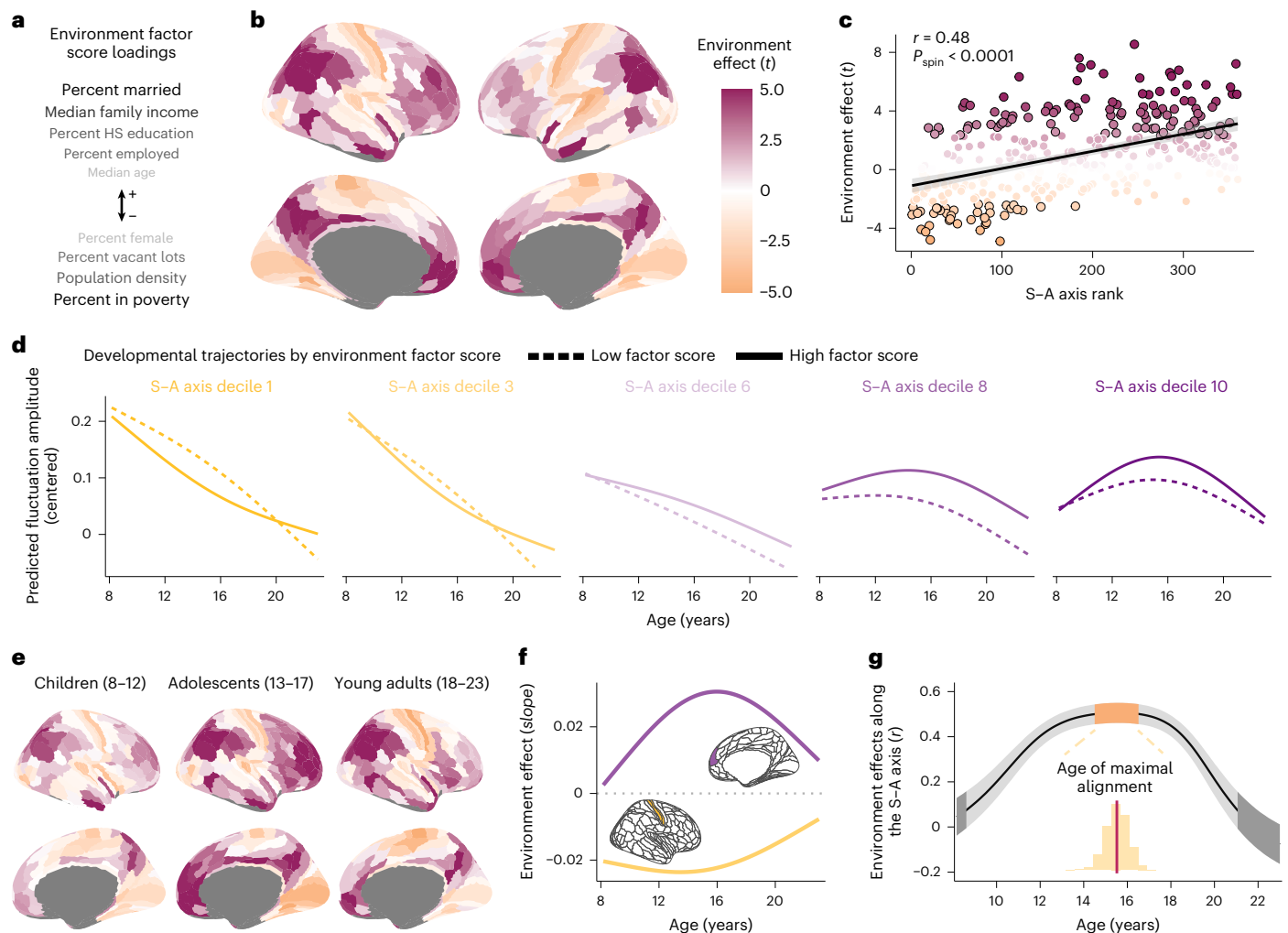
Fig. 6 | Associations between fluctuation amplitude and the developmental environment vary along the S–A axis in adolescence. a, An environment factor score captures multiple features of each child's neighborhood environment. Variables listed above (+) and below (−) the arrow positively and negatively loaded onto the factor score, respectively. Darker and larger text indicates stronger loadings. Higher factor scores reflect greater neighborhood-level socioeconomic advantage; HS, high school. **b**, A cortical map displaying regional associations (quantified by model *t* values) between environment factor scores and fluctuation amplitude is displayed; the map partly recapitulates the S–A axis. **c**, Each region's environment effect (*t* value) is plotted against its S–A axis rank (linear fit shown with a 95% confidence interval). Regions with a significant environment effect following correction for multiple comparisons are outlined in black. The S–A axis explains significant variability in brain–environment associations (Spearman's correlation with a spatial rotation-based significance test: *r* = 0.48 and P_{spin} < 0.0001). **d**, Fluctuation amplitude developmental trajectories are displayed for low and high environment factor scores for five deciles of the S–A axis, illustrating environment-associated differences in

this measure by developmental timing. **e**, Cortical maps depicting regional associations between environment factor scores and fluctuation amplitude (as in **b**) in child, adolescent and young-adult groups show subtle differences in associations throughout development. Magenta and orange denote positive and negative environment effects (*t* values), respectively, as in **b**. **f**, Age-specific environment effects are shown for an exemplar primary sensorimotor region (primary somatosensory cortex area 3b; yellow) and transmodal association region (medial prefrontal cortex area 9m; purple). The magnitude of effects is largest in adolescence in these regions. **g**, Regional differences in environment associations are most organized along the S–A axis in adolescence, as revealed by age-specific correlations between regional environment effects and S–A axis ranks. The plot depicts the median correlation value (*r*) at each age (black line) and the 95% credible interval around this value (gray band) obtained by sampling the posterior distribution of regional age-by-environment interaction GAMs 10,000 times. The orange and dark gray bands respectively designate credible intervals for the ages of maximal and zero correlation of environment effects with the S–A axis.

neighborhood socioeconomic environment were summarized using a single previously published factor score[47]. Higher factor scores indicate that an individual lived in a neighborhood with a higher median family income, lower population density, fewer vacant housing lots, a greater percentage of residents who are married, employed and high school educated and a lower percentage of residents in poverty (Fig. 6a). We focused on the neighborhood environment specifically, as the factor score robustly aggregates across a wide range of measures related to the physical, social and cognitive environment, captures socioeconomic inequality at the societal and systems

levels and has been shown to account for individual differences in brain function and behavior beyond the household environment[47,48].

We first modeled linear associations between neighborhood environment factor scores and regional fluctuation amplitude using GAMs while controlling for developmental effects (age) and other covariates (in-scanner motion and sex). Forty-two percent of cortical regions showed a significant association between fluctuation amplitude and the neighborhood environment (P_{FDR} < 0.05 in 141 regions). Higher environment factor scores were associated with higher fluctuation amplitude across the association cortex, but with lower fluctuation amplitude

nearly exclusively within primary and early sensory and motor cortices (Fig. 6b). This pattern of relationships indicates that youth raised in neighborhoods with higher income, education and employment rates and with lower population density and poverty tended to have greater-amplitude intrinsic fMRI fluctuations in higher-order cortices and lower-amplitude fluctuations in modality-specific cortices. Strikingly, environment effects and S–A axis ranks were significantly correlated across the cortical mantle ($r = 0.48$, $P_{spin} < 0.0001$; Fig. 6c), establishing that variation in associations between the neighborhood environment and intrinsic fMRI activity amplitude is expressed along the brain's global cortical hierarchy. We attempted to statistically disambiguate between the influence of the neighborhood environment and household socioeconomic position by controlling environment factor score GAMs for parental education, one indicator of individual socioeconomic status. In this specificity analysis, the association between neighborhood environment factor scores and fluctuation amplitude remained significant ($P_{FDR} < 0.05$) in 101 of the original 141 regions, and regional environment effects still significantly varied along the S–A axis ($r = 0.54$, $P_{spin} < 0.0001$). Conversely, there were no significant associations between parental education and fluctuation amplitude (all $P_{FDR} > 0.05$), supporting a potentially stronger role for neighborhood-level (dis)advantage rather than household socioeconomic position.

To better appreciate the nature of associations between the neighborhood environment and fMRI activity amplitude from a developmental perspective, we modeled age-dependent changes in fluctuation amplitude as a function of environment factor score. We visualized developmental trajectories for low and high environment factor scores for deciles of the S–A axis (stratifying Fig. 3c by factor score). A higher neighborhood environment factor score (indicative of more advantaged socioeconomic circumstances) was associated with a steeper reduction in fluctuation amplitude in sensorimotor regions (deciles 1 and 3) during childhood and adolescence and with a greater peak in fluctuation amplitude in association regions (deciles 8 and 10) particularly during midadolescence (Fig. 6d). Factor score-stratified developmental trajectories thus suggested that environment effects may be largest and most divergent between sensorimotor and association cortices during adolescence.

To study this possibility further, we divided the sample into child (8–12 years), adolescent (13–17 years) and young-adult (18–23 years) groups and quantified regional associations between environment factor scores and fluctuation amplitude at each developmental stage. Regional environment effect estimates were quite correlated across the three groups, suggesting relative stability in associations across development ($r = 0.72$ between child and adolescent t values, $r = 0.70$ between adolescent and young-adult t values, and $r = 0.65$ between child and young-adult t values). However, small differences in regional associations were present across developmental stages (Fig. 6e) and together resulted in environment effect estimates becoming most strongly differentiated across the S–A axis in adolescence. The correlation between regional environment effects and S–A axis ranks was $r = 0.32$ ($P_{spin} = 0.00765$) in children, $r = 0.65$ ($P_{spin} < 0.0001$) in adolescents and $r = 0.31$ ($P_{spin} = 0.01280$) in young-adults.

Given initial evidence that developmental timing may affect the global expression of brain–environment associations, we used GAMs to formally model regional age-by-environment interactions, which estimate how relationships between environment factor scores and fluctuation amplitude vary continuously with age. This approach allowed for the derivation of age-specific environment effect estimates, providing insight into how the magnitude of effects changed over the developmental window studied in individual sensorimotor and association regions (Fig. 6f). Moreover, this approach facilitated a second age-resolved analysis in which we calculated the correlation between age-specific environment effects and S–A axis ranks at 1-month intervals between ages 8 and 23 years (Fig. 6g). The goal of this second age-resolved analysis was to investigate whether subtle

changes in regional environment effects contribute to a shift in the global patterning of brain–environment associations with age. This analysis revealed that regional environment effects and regional S–A axis ranks were maximally correlated in adolescence at 15.5 years of age (95% credible interval of 14.4 to 16.6 years), providing convergent results to the grouped developmental stage analysis. The spatial correlation between environment effects and the S–A axis did not significantly differ from 0 at the very youngest (<8.8 years old) and oldest (>21.0 years old) ages studied. These results collectively suggest that the expression of brain–environment associations along this principal axis of brain organization is most prominent in adolescence.

Discussion

During embryonic and early postnatal cortical development, developmental programs are spatially and temporally governed by major organizing axes. Cortical arealization is cooperatively controlled by thalamocortical inputs and transcription factors expressed along anterior–medial to posterior–lateral axes[49]. Neurogenesis terminates along an anterior to posterior axis[50]. The alignment of developmental programs with neuroaxes is thus a fundamental element of early cortical development. In the current study, we demonstrate that the maturation of intrinsic cortical activity conforms to the hierarchical S–A axis from ages 8 to 18 years, supporting that this core facet of development extends to childhood and adolescence. Specifically, we observed that declines in the amplitude of intrinsic fMRI activity are temporally coupled to the increasing expression of a plasticity-limiting factor and temporally staggered along the S–A axis of cortical organization. We additionally found that the S–A axis captures not only interregional variation in maturational profiles but also variation in the effects of children's developmental environment on cortical fMRI activity. Together, these results provide evidence of a hierarchical axis of neurodevelopment in youth.

Intrinsic neural activity has a profound influence on the immature brain, impacting neuron survival, circuit wiring, topographic map formation, synaptic connectivity and overall cortical volume[18,51–53]. Prominent changes in the prevalence and patterning of this activity occur during development, engendered by shifts in the maturity of the cortex and in the level of cortical plasticity. Here, we identified prolonged declines in fMRI fluctuation amplitude, an in vivo measure sensitive to intrinsic cortical activity, throughout the protracted course of human neurodevelopment. Moreover, we observed substantial interregional heterochronicity in periods of decline, with fluctuation amplitude beginning to decline around 8–12 years of age in unimodal sensory and motor regions, 13–16 years in many association cortices and 18–22 years in prefrontal transmodal cortices. These region-specific windows of declining fluctuation amplitude occur after peak gray matter volume is obtained[5] and coincide with regional windows of extensive synaptic pruning[10]. In addition, we demonstrated that each region's onset of decline in fluctuation amplitude was linked to its period of maximal increase in a non-invasive measure of intracortical myelin growth. Maturational refinement of this functional measure is thus temporally linked to developmental changes in multiple indicators of shifting circuit plasticity, suggesting the presence of a graded axis of neurodevelopmental plasticity during childhood and adolescence.

Indeed, in support of our proposed framework on developmental chronology[4], we found that regional differences in maturational profiles were systematically explained by the asynchronous patterning of developmental change across the S–A axis. Regional developmental trajectories diverged in a continuous fashion across this axis, in a manner that suggests that a maturational sequence progresses along the brain's cortical hierarchy with age. This underscores that the S–A axis can be considered both a dominant spatial feature axis and a primary neurodevelopmental axis and intimates that spatial feature variability may in part emerge from temporal developmental variability[4,50]. Recent work has shown that cortical microstructure[9] and functional

connectivity[7] increasingly differentiate across the S–A axis during late childhood and adolescence, when development is maximally organized by this axis. Hence, one main outcome of hierarchical development may be the strengthening of variation along the S–A axis, with a consequent strengthening of the cortex's hierarchical topography[4].

Although this non-invasive imaging study could not establish the mechanisms underlying the sensorimotor-to-associative sequence of fMRI activity refinement, prior work suggests that it may be produced by the hierarchical maturation of plasticity-regulating structural and chemical features. Key plasticity-regulating processes include the growth of intracortical myelin[25,54], the strengthening of parvalbumin interneuron signaling[24,54] and the assembly of perineuronal nets[17,55]. These processes elicit transitions in the prevalence, synchronicity and recorded amplitude of spontaneous activity[17,23,44,56], indicating that they could possibly contribute to developmental changes in fMRI activity amplitude. In the adult cortex, the cortical distribution of parvalbumin interneurons is coupled to regional differences in fMRI fluctuation amplitude, with parvalbumin interneuron-associated genes accounting for an enriched degree of heritable variance in this measure[56]. In the developing cortex, cortical myelin and perineuronal nets preferentially form around parvalbumin interneurons[17,55,57], limiting developmental plasticity while simultaneously altering a circuit's excitation:inhibition ratio and the production of intrinsic activity[11,54]. Critically, it has been established that cortical myelin[8,42] and parvalbumin interneurons[11,16,58] mature earlier in sensory cortices and later in association cortices, indicating that their temporal development parallels the developmental reductions in the amplitude of intrinsic fMRI activity characterized here. The amplitude of intrinsic fMRI activity also uniquely increased in transmodal cortices in adolescence (frequently until 13–17 years), suggesting that a functional signature of more highly malleable cortices increases in association areas in this developmental window. The neurobiological events that could contribute to potential late increases in association cortex plasticity in the human brain have yet to be identified. Candidate events identified in animal studies include slower degradation of molecules that can delay the onset of plasticity (for example, polysialic acid[54] and histone deacetylases[16]) or late increases in plasticity facilitators (for example, brain-derived neurotrophic factor[54], thalamocortical inputs[59] and homeoprotein Otx2 (ref. [54])).

It has been hypothesized that age-dependent changes in the distribution of cortical plasticity should allow the same external inputs to exert differential influences on the human brain, depending on developmental timing. The present work provides empirical support for this hypothesis. Specifically, we studied relationships between individual differences in intrinsic activity amplitude and environment factor scores; these scores index disparities in neighborhood-level socioeconomic conditions that should be recognized as a manifestation of systemic wealth and education inequity that is rooted in structural racism and racial inequity[60]. We found that youth living in neighborhoods with greater poverty, unemployment rates and population density exhibited reduced fluctuation amplitude across the association cortex—most prominently, a reduced peak in amplitude in transmodal cortex during midadolescence. Yet, youth from more disadvantaged environments also had higher-amplitude intrinsic fMRI activity in unimodal sensory and motor cortices. Together, these opposing environment effects in sensorimotor and association cortices indicate that greater environmental deprivation is associated with diminished differentiation of a putative functional plasticity signature across the maturing cortex. We speculate that this association could reflect reduced versus accelerated development of plasticity-restricting features such as myelin in sensorimotor and association cortices, respectively, in youth from poorer socioeconomic environments[61].

Importantly, the cortical expression of brain–environment associations was not uniform across the entire age range studied. An age-resolved analysis revealed that environment effects diverged most between sensorimotor and association cortices during adolescence, coincident with when regional differences in developmental change were most hierarchically organized. In fact, both developmental and environmental effects exhibited maximal variation across the cortex's S–A axis at 15 years of age. This temporal concurrence uncovers interdependence between ongoing neurodevelopmental refinement and environmental influences, revealing how the effects of the environment on the youth brain depend on developmental stage. Our analyses of youths' neighborhood environments thus provide data consistent with the hypothesis that environmental influences are both sensitive to and capable of refining a cortical area's current developmental plastic state.

Several limitations and possible direct extensions of this work should be highlighted. First, this was a cross-sectional investigation of neurodevelopment in youth. Future investigations with longitudinal study designs could characterize within-individual changes in cortical intrinsic activity and the effects of the environment on the pace of an individual's development. Longitudinal studies will also be better suited to examine temporal precedence between developmental refinement of intrinsic fMRI activity and maturation of plasticity-regulating features. Second, we used resting-state fMRI to study intrinsic cortical activity; however, the BOLD signal is sensitive to neural, vascular and respiratory factors. While sensitivity analyses aimed at assessing and mitigating these factors provided highly convergent results, future studies using more direct measures of neural activity will therefore be helpful for extending the present findings. Third, it is difficult to directly establish the extent to which age-related changes in non-invasive neuroimaging measures represent changes in developmental plasticity versus other processes, given that there is no gold standard or singular measure of cortical plasticity in the human brain. To address this challenge, we studied an fMRI-derived measure that is modulated by changing the activity of cells that drive developmental plasticity[16,34,56], is enhanced by behaviorally inducing plasticity[33,35] and, as shown here, appears to be refined during development in tandem with a biological regulator of plasticity. Fourth, only a coarse measure of pubertal stage was available in this sample, and it was only collected in individuals 10 years of age and older. This limited our ability to fully ascertain whether regional fluctuation amplitude was influenced by puberty or hormone levels, especially in the youngest participants. Rodent studies have shown that pubertal hormones can affect synaptic pruning and inhibitory signaling in the association cortex[62], highlighting this as an area for further investigation. Fifth, we aggregated a set of interrelated neighborhood variables into one factor score, precluding inference about specific proximal or distal causes of the brain–environment associations observed in these data. Potential causes may involve neighborhood features that are socioeconomically stratified and sociopolitically determined, including access to physical and educational resources, exposure to environmental enrichment and community programs or experiences of psychological safety and chronic stress. Developing a more nuanced understanding of the causes and behavioral correlates of these environment effects may ultimately help to inform interventions or policies that equitably support healthy child neurodevelopment across socioeconomic circumstances.

The present study demonstrates that during childhood and adolescence, the spatiotemporal patterning of developmental change in intrinsic cortical fMRI activity coheres with a hierarchical axis of cortical organization. The observed refinements in fMRI fluctuations lend support to the theory that shifts in circuit plasticity temporally progress along this axis, calling for studies that can mechanistically test for neurobiological events driving an S–A gradient of neurodevelopment. Such events may include the maturation of neurochemical and structural plasticity-regulating features and successive expression of molecules that can orchestrate developmental timing, for example, circadian clock genes and temporally organized transcription factors[16,63,64]. Given the relevance of the S–A axis for understanding cortical development in childhood and adolescence, future work should explore whether this and other major organizing axes (for example, anatomical axes)

play a role in cortical refinement during infancy and early childhood. Studies of the infant brain have shown that developmental change in thalamocortical structural connectivity and cortico-cortical functional connectivity is more pronounced within the sensorimotor cortex than within the association cortex, suggesting maturational relevance of the S–A axis in the first years of life[65]. Continued discovery of temporal axes of neurodevelopment across the multidecade maturational course of humans will help elucidate how plasticity is distributed across brain regions at different developmental stages. Such insights into the temporal progression of plasticity will facilitate an understanding of how the effects of experience and the environment on the brain change as cortical malleability is refined, and may thus ultimately help to guide interventions in youth that align with each child's neurotemporal context.

Online content

Any methods, additional references, Nature Portfolio reporting summaries, source data, extended data, supplementary information, acknowledgements, peer review information; details of author contributions and competing interests; and statements of data and code availability are available at https://doi.org/10.1038/s41593-023-01282-y.

References

1. Sydnor, V. J. & Satterthwaite, T. D. Neuroimaging of plasticity mechanisms in the human brain: from critical periods to psychiatric conditions. *Neuropsychopharmacology* **48**, 219–220 (2023).
2. Cooper, E. A. & Mackey, A. P. Sensory and cognitive plasticity: implications for academic interventions. *Curr. Opin. Behav. Sci.* **10**, 21–27 (2016).
3. Sisk, L. M. & Gee, D. G. Stress and adolescence: vulnerability and opportunity during a sensitive window of development. *Curr. Opin. Psychol.* **44**, 286–292 (2022).
4. Sydnor, V. J. et al. Neurodevelopment of the association cortices: patterns, mechanisms, and implications for psychopathology. *Neuron* **109**, 2820–2846 (2021).
5. Bethlehem, R. A. I. et al. Brain charts for the human lifespan. *Nature* **604**, 525–533 (2022).
6. Gogtay, N. et al. Dynamic mapping of human cortical development during childhood through early adulthood. *Proc. Natl Acad. Sci. USA* **101**, 8174–8179 (2004).
7. Dong, H.-M., Margulies, D. S., Zuo, X.-N. & Holmes, A. J. Shifting gradients of macroscale cortical organization mark the transition from childhood to adolescence. *Proc. Natl Acad. Sci. USA* **118**, e2024448118 (2021).
8. Grydeland, H. et al. Waves of maturation and senescence in micro-structural mri markers of human cortical myelination over the lifespan. *Cereb. Cortex* **29**, 1369–1381 (2019).
9. Paquola, C. et al. Shifts in myeloarchitecture characterise adolescent development of cortical gradients. *eLife* **8**, e50482 (2019).
10. Huttenlocher, P. R. & Dabholkar, A. S. Regional differences in synaptogenesis in human cerebral cortex. *J. Comp. Neurol.* **387**, 167–178 (1997).
11. Larsen, B. & Luna, B. Adolescence as a neurobiological critical period for the development of higher-order cognition. *Neurosci. Biobehav. Rev.* **94**, 179–195 (2018).
12. García-Cabezas, M. Á., Zikopoulos, B. & Barbas, H. The structural model: a theory linking connections, plasticity, pathology, development and evolution of the cerebral cortex. *Brain Struct. Funct.* **224**, 985–1008 (2019).
13. Huntenburg, J. M., Bazin, P.-L. & Margulies, D. S. Large-scale gradients in human cortical organization. *Trends Cogn. Sci.* **22**, 21–31 (2018).
14. Margulies, D. S. et al. Situating the default-mode network along a principal gradient of macroscale cortical organization. *Proc. Natl Acad. Sci. USA* **113**, 12574–12579 (2016).
15. Hilgetag, C. C., Goulas, A. & Changeux, J.-P. A natural cortical axis connecting the outside and inside of the human brain. *Netw. Neurosci.* **6**, 950–959 (2022).
16. Reh, R. K. et al. Critical period regulation across multiple timescales. *Proc. Natl Acad. Sci. USA* **117**, 23242–23251 (2020).
17. Lensjø, K. K., Lepperød, M. E., Dick, G., Hafting, T. & Fyhn, M. Removal of perineuronal nets unlocks juvenile plasticity through network mechanisms of decreased inhibition and increased gamma activity. *J. Neurosci.* **37**, 1269–1283 (2017).
18. Martini, F. J., Guillamón-Vivancos, T., Moreno-Juan, V., Valdeolmillos, M. & López-Bendito, G. Spontaneous activity in developing thalamic and cortical sensory networks. *Neuron* **109**, 2519–2534 (2021).
19. Frye, C. G. & MacLean, J. N. Spontaneous activations follow a common developmental course across primary sensory areas in mouse neocortex. *J. Neurophysiol.* **116**, 431–437 (2016).
20. Golshani, P. et al. Internally mediated developmental desynchronization of neocortical network activity. *J. Neurosci.* **29**, 10890–10899 (2009).
21. Nakazawa, S., Yoshimura, Y., Takagi, M., Mizuno, H. & Iwasato, T. Developmental phase transitions in spatial organization of spontaneous activity in postnatal barrel cortex layer 4. *J. Neurosci.* **40**, 7637–7650 (2020).
22. Toyoizumi, T. et al. A theory of the transition to critical period plasticity: inhibition selectively suppresses spontaneous activity. *Neuron* **80**, 51–63 (2013).
23. Chini, M., Pfeffer, T. & Hanganu-Opatz, I. An increase of inhibition drives the developmental decorrelation of neural activity. *eLife* **11**, e78811 (2022).
24. Fagiolini, M. & Hensch, T. K. Inhibitory threshold for critical-period activation in primary visual cortex. *Nature* **404**, 183–186 (2000).
25. McGee, A. W., Yang, Y., Fischer, Q. S., Daw, N. W. & Strittmatter, S. M. Experience-driven plasticity of visual cortex limited by myelin and Nogo receptor. *Science* **309**, 2222–2226 (2005).
26. Laumann, T. O. & Snyder, A. Z. Brain activity is not only for thinking. *Curr. Opin. Behav. Sci.* **40**, 130–136 (2021).
27. Luhmann, H. J. et al. Spontaneous neuronal activity in developing neocortical networks: from single cells to large-scale interactions. *Front. Neural Circuits* **10**, 40 (2016).
28. Lake, E. M. R. et al. Simultaneous cortex-wide fluorescence Ca^{2+} imaging and whole-brain fMRI. *Nat. Methods* **17**, 1262–1271 (2020).
29. Ma, Z., Zhang, Q., Tu, W. & Zhang, N. Gaining insight into the neural basis of resting-state fMRI signal. *NeuroImage* **250**, 118960 (2022).
30. Magri, C., Schridde, U., Murayama, Y., Panzeri, S. & Logothetis, N. K. The amplitude and timing of the BOLD signal reflects the relationship between local field potential power at different frequencies. *J. Neurosci.* **32**, 1395–1407 (2012).
31. Shmuel, A. & Leopold, D. A. Neuronal correlates of spontaneous fluctuations in fMRI signals in monkey visual cortex: implications for functional connectivity at rest. *Hum. Brain Mapp.* **29**, 751–761 (2008).
32. Yu-Feng, Z. et al. Altered baseline brain activity in children with ADHD revealed by resting-state functional MRI. *Brain Dev.* **29**, 83–91 (2007).
33. Fair, D. A. & Yeo, B. T. T. Precision neuroimaging opens a new chapter of neuroplasticity experimentation. *Neuron* **107**, 401–403 (2020).
34. Markicevic, M. et al. Cortical excitation:inhibition imbalance causes abnormal brain network dynamics as observed in neurodevelopmental disorders. *Cereb. Cortex* **30**, 4922–4937 (2020).
35. Newbold, D. J. et al. Plasticity and spontaneous activity pulses in disused human brain circuits. *Neuron* **107**, 580–589 (2020).
36. Hinton, E. A., Li, D. C., Allen, A. G. & Gourley, S. L. Social isolation in adolescence disrupts cortical development and

36. goal-dependent decision-making in adulthood, despite social reintegration. *eNeuro* **6**, ENEURO.0318-19.2019 (2019).

37. Greifzu, F. et al. Environmental enrichment extends ocular dominance plasticity into adulthood and protects from stroke-induced impairments of plasticity. *Proc. Natl Acad. Sci. USA* **111**, 1150–1155 (2014).

38. Favuzzi, E. et al. Activity-dependent gating of parvalbumin interneuron function by the perineuronal net protein brevican. *Neuron* **95**, 639–655 (2017).

39. Tooley, U. A., Bassett, D. S. & Mackey, A. P. Environmental influences on the pace of brain development. *Nat. Rev. Neurosci.* **22**, 372–384 (2021).

40. Colich, N. L., Rosen, M. L., Williams, E. S. & McLaughlin, K. A. Biological aging in childhood and adolescence following experiences of threat and deprivation: a systematic review and meta-analysis. *Psychol. Bull.* **146**, 721–764 (2020).

41. McDermott, C. L. et al. Early life stress is associated with earlier emergence of permanent molars. *Proc. Natl Acad. Sci. USA* **118**, e2105304118 (2021).

42. Baum, G. L. et al. Graded variation in T1w/T2w ratio during adolescence: measurement, caveats, and implications for development of cortical myelin. *J. Neurosci.* **42**, 5681–5694 (2022).

43. de Faria, O. et al. Periods of synchronized myelin changes shape brain function and plasticity. *Nat. Neurosci.* **24**, 1508–1521 (2021).

44. Kato, D. et al. Motor learning requires myelination to reduce asynchrony and spontaneity in neural activity. *Glia* **68**, 193–210 (2020).

45. Burt, J. B. et al. Hierarchy of transcriptomic specialization across human cortex captured by structural neuroimaging topography. *Nat. Neurosci.* **21**, 1251–1259 (2018).

46. Hill, J. et al. Similar patterns of cortical expansion during human development and evolution. *Proc. Natl Acad. Sci. USA* **107**, 13135–13140 (2010).

47. Moore, T. M. et al. Characterizing social environment's association with neurocognition using census and crime data linked to the Philadelphia Neurodevelopmental Cohort. *Psychol. Med.* **46**, 599–610 (2016).

48. Tooley, U. A. et al. Associations between neighborhood SES and functional brain network development. *Cereb. Cortex* **30**, 1–19 (2020).

49. O'Leary, D. D. M., Chou, S.-J. & Sahara, S. Area patterning of the mammalian cortex. *Neuron* **56**, 252–269 (2007).

50. Charvet, C. J. & Finlay, B. L. Evo-devo and the primate isocortex: the central organizing role of intrinsic gradients of neurogenesis. *Brain Behav. Evol.* **84**, 81–92 (2014).

51. Ackman, J. B., Burbridge, T. J. & Crair, M. C. Retinal waves coordinate patterned activity throughout the developing visual system. *Nature* **490**, 219–225 (2012).

52. Benders, M. J. et al. Early brain activity relates to subsequent brain growth in premature infants. *Cereb. Cortex* **25**, 3014–3024 (2015).

53. Winnubst, J., Cheyne, J. E., Niculescu, D. & Lohmann, C. Spontaneous activity drives local synaptic plasticity in vivo. *Neuron* **87**, 399–410 (2015).

54. Takesian, A. E. & Hensch, T. K. in *Progress in Brain Research*, Vol. 207 (eds. Merzenich, M. M., Nahum, M. & Van Vleet, T. M.) Ch. 1 (Elsevier, 2013).

55. Carulli, D. et al. Animals lacking link protein have attenuated perineuronal nets and persistent plasticity. *Brain* **133**, 2331–2347 (2010).

56. Anderson, K. M. et al. Transcriptional and imaging-genetic association of cortical interneurons, brain function, and schizophrenia risk. *Nat. Commun.* **11**, 2889 (2020).

57. Micheva, K. D. et al. A large fraction of neocortical myelin ensheathes axons of local inhibitory neurons. *eLife* **5**, e15784 (2016).

58. Condé, F., Lund, J. S. & Lewis, D. A. The hierarchical development of monkey visual cortical regions as revealed by the maturation of parvalbumin-immunoreactive neurons. *Brain Res. Dev. Brain Res.* **96**, 261–276 (1996).

59. Benoit, L. J. et al. Adolescent thalamic inhibition leads to long-lasting impairments in prefrontal cortex function. *Nat. Neurosci.* **25**, 714–725 (2022).

60. Acevedo-Garcia, D. et al. Racial and ethnic inequities in children's neighborhoods: evidence from the new child opportunity index 2.0. *Health Aff.* **39**, 1693–1701 (2020).

61. Norbom, L. B. et al. Parental socioeconomic status is linked to cortical microstructure and language abilities in children and adolescents. *Dev. Cogn. Neurosci.* **56**, 101132 (2022).

62. Piekarski, D. J., Boivin, J. R. & Wilbrecht, L. Ovarian hormones organize the maturation of inhibitory neurotransmission in the frontal cortex at puberty onset in female mice. *Curr. Biol.* **27**, 1735–1745 (2017).

63. Kobayashi, Y., Ye, Z. & Hensch, T. K. Clock genes control cortical critical period timing. *Neuron* **86**, 264–275 (2015).

64. Konstantinides, N. et al. A complete temporal transcription factor series in the fly visual system. *Nature* **604**, 316–322 (2022).

65. Nielsen, A. N. et al. Maturation of large-scale brain systems over the first month of life. *Cereb. Cortex* https://doi.org/10.1093/cercor/bhac242 (2022).

[1]Penn Lifespan Informatics and Neuroimaging Center (PennLINC), Perelman School of Medicine, University of Pennsylvania, Philadelphia, PA, USA. [2]Department of Psychiatry, Perelman School of Medicine, University of Pennsylvania, Philadelphia, PA, USA. [3]Department of Child and Adolescent Psychiatry and Behavioral Science, The Children's Hospital of Philadelphia, Philadelphia, PA, USA. [4]Penn–CHOP Lifespan Brain Institute, Perelman School of Medicine, Children's Hospital of Philadelphia, Philadelphia, PA, USA. [5]Department of Bioengineering, School of Engineering and Applied Science, University of Pennsylvania, Philadelphia, PA, USA. [6]Department of Electrical and Systems Engineering, School of Engineering and Applied Science, University of Pennsylvania, Philadelphia, PA, USA. [7]Department of Physics and Astronomy, College of Arts and Sciences, University of Pennsylvania, Philadelphia, PA, USA. [8]Department of Neurology, Perelman School of Medicine, University of Pennsylvania, Philadelphia, PA, USA. [9]Santa Fe Institute, Santa Fe, NM, USA. [10]Department of Radiology, Perelman School of Medicine, University of Pennsylvania, Philadelphia, PA, USA. [11]Center for Biomedical Image Computing and Analytics, University of Pennsylvania, Philadelphia, PA, USA. [12]Department of Psychology, University of Pennsylvania, Philadelphia, PA, USA. [13]Penn Statistics in Imaging and Visualization Endeavor (PennSIVE), Perelman School of Medicine, University of Pennsylvania, Philadelphia, PA, USA. [14]Department of Biostatistics, Epidemiology and Informatics, Perelman School of Medicine, University of Pennsylvania, Philadelphia, PA, USA. ✉e-mail: sattertt@pennmedicine.upenn.edu

Methods

Participants

Participants were recruited as part of the Philadelphia Neurodevelopmental Cohort[66], a community study of child and adolescent brain development. Demographic, clinical, environmental and neuroimaging data from 1,033 youths were included in the present cross-sectional study. Study sample demographics include an age range of 8 to 23 years (mean age of 15.7 ± 3.3 years), a sex distribution of 467 males and 566 females (sex was self-reported; intersex was not assessed) and a race and ethnicity distribution that was 0.3% American Indian or Alaskan Native, 0.7% Asian, 41% Black or African American, 11% identifying as multiracial and 47% White. All participants over the age of 18 gave written informed consent before study participation. Participants under the age of 18 gave informed assent with written parental consent. All individuals received monetary compensation for participation in the study. All study procedures were approved by the Institutional Review Boards of the University of Pennsylvania and the Children's Hospital of Philadelphia.

MRI data acquisition

T1w structural MRI and resting-state fMRI data were used in the present study. All MRI scans were acquired on the same 3T Siemens TIM Trio scanner (software version VB17) at the University of Pennsylvania with a 32-channel head coil. T1w structural images were acquired with a magnetization-prepared rapid acquisition gradient-echo sequence with the following parameters: repetition time of 1,810 ms, echo time of 3.51 ms, inversion time of 1,100 ms, flip angle of 9°, field of view of 180 × 240 mm, matrix of 192 × 256, 160 slices and a voxel resolution of 0.94 × 0.94 × 1 mm. Resting-state functional images were acquired with a single-shot, interleaved multislice gradient-echo echo planar imaging sequence with the following parameters: repetition time of 3 s, echo time of 32 ms, flip angle of 90°, field of view of 192 × 192 mm, matrix of 64 × 64, 46 slices, a voxel resolution of 3 mm³ and 124 volumes. To enable susceptibility distortion correction of resting-state functional images, a map of the main magnetic field (a B0 field map) was additionally collected using a dual-echo, gradient-recalled echo (GRE) sequence with the following parameters: repetition time of 1,000 ms, echo time 1 of 2.69 ms, echo time 2 of 5.27 ms, flip angle of 60°, field of view of 240 × 240 mm, matrix of 64 × 64, 44 slices and a voxel resolution of 3.8 × 3.8 × 4 mm.

MRI data processing

T1w images and resting-state fMRI time series were processed with fMRIPrep 20.2.3 (ref. [67]). The T1w image was corrected for intensity non-uniformity with Advanced Normalization Tools[68] (ANTs; 2.3.3) N4BiasFieldCorrection, the skull was stripped with a Nipype (1.6.1) implementation of the ANTs brain extraction workflow, and tissue segmentation was performed with FSL (5.0.9) fast. The processed T1w image was then used for cortical surface reconstruction with FreeSurfer (6.0.1)[69]. The T1w image was additionally non-linearly registered to the MNI152 T1 template (volume-based spatial normalization) with antsRegistration.

To preprocess functional scans, a skull-stripped reference BOLD volume was first generated, and a B0 field map was co-registered to this reference volume. The B0 field map was estimated based on the phase-difference map calculated with the dual-echo GRE sequence, converted to a displacements field map with FSL's fugue and SDCflow tools and used for susceptibility distortion correction of the reference BOLD volume. The susceptibility-corrected BOLD reference was then rigidly co-registered (6 degrees of freedom) to the T1 reference using boundary-based registration implemented with FreeSurfer's bbregister. The fMRI time series were slice-time corrected using 3dTshift from AFNI 20160207 and resampled onto their original native space by applying a single composite transform to correct for susceptibility distortions and in-scanner head motion. Head motion parameters

pubertal stage, we added a three-level ordered factor for pubertal stage (with levels for prepubertal, midpubertal and postpubertal) to the main GAM models. Participants self-reported their pubertal stage by viewing pictorial representations and text descriptions of the five Tanner stages of pubic hair growth and reporting which best matched their own development of secondary sex characteristics. Following our prior work in this same sample[79], we considered Tanner stages 1–3 as 'prepubertal', Tanner stage 4 as 'midpubertal' and Tanner stage 5 as 'postpubertal'. Self-reporting of Tanner staging was only conducted in participants aged 10 and older (n = 949; 518 female). As a result, there were fewer prepubertal participants (n = 176, Tanner stages 1–3) than midpubertal (n = 283, Tanner stage 4) and postpubertal (n = 490, Tanner stage 5) participants. We evaluated whether pubertal stage explained significant variance in fluctuation amplitude above and beyond age in each region by using an ANOVA to compare the full GAM model (with the pubertal stage factor) to a reduced model that did not include pubertal information. We corrected P values for multiple comparisons across region-wise GAMs within sex and pubertal stage analyses using FDR correction.

Associations with cortical myelin development. We formally assessed whether the development of intrinsic fMRI activity amplitude was spatially and temporally related to the development of an imaging measure sensitive to intracortical myelin content. Cortical myelin development was previously comprehensively characterized by Baum et al.[42] using T1w/T2w surface-based myelin mapping in a sample of 628 youths ages 8 to 21 years (336 female) who had data collected as part of the HCP in Development. Using high-resolution (0.8-mm³) T1w and T2w images, HCP processing pipelines and state of the art methods for B_1^+ transmit field bias correction and partial volume reduction, Baum et al.[42] investigated the maturational trajectory of increases in the T1w/T2w ratio in each cortical region. In this investigation, the authors fit region-specific GAMs with a smooth term for age using thin plate regression splines as the smoothing basis, paralleling the present work. GAMs included covariates for sex, scanner and B_1^+ transmit field correction-related variables, following current best practices for statistically comparing the T1w/T2w ratio across individuals.

To test whether the extent to which fluctuation amplitude changed with age was related to the degree to which cortical myelin content changed with age, we calculated the correlation coefficient between the two distinct age effects: those calculated from regional fluctuation amplitude GAMs and those calculated from regional T1w/T2w ratio GAMs reported by Baum et al.[42]. As in the present work, T1w/T2w ratio age effects were determined by a partial R^2 derived by comparing the full GAM model to a reduced model with no smooth term for age. The association between fluctuation amplitude age effects and T1w/T2w ratio age effects was quantified with a Spearman's correlation, a non-parametric, rank-based correlation test that does not assume normality. A Spearman's correlation was also used to evaluate whether there was temporal correspondence between the development of fluctuation amplitude and the T1w/T2w ratio across the cortex. Specifically, we calculated the correlation coefficient between the age at which fluctuation amplitude began to significantly decrease in each region and the age at which the T1w/T2w ratio maximally increased in each region. The age at which fluctuation amplitude began to significantly decrease was the youngest age at which the first derivative of the age smooth function was significantly negative. The age at which the T1w/T2w ratio had a maximal rate of increase was the age at which the first derivative of the age smooth function was maximal.

Alignment with the S–A axis. This work sought to test the overarching hypothesis that neurodevelopmental patterns are organized by the S–A axis during childhood and adolescence. We therefore examined whether fluctuation amplitude maturation aligned with the S–A axis derived in our prior work[4]. The S–A axis was derived by averaging

were calculated with respect to the reference BOLD volume before any spatiotemporal filtering using FSL mcflirt; six rotation and translation parameters were calculated. BOLD time series were additionally resampled into standard space, generating preprocessed time series in the MNI152NLin6Asym T1 template, and onto the fsaverage surface. Finally, to project functional time series onto the fsLR cortical surface for study analyses, grayordinates files containing 32,000 vertices per hemisphere were generated using the highest-resolution fsaverage as an intermediate standardized surface space. Volumetric resampling was performed using antsApplyTransforms configured with Lanczos interpolation to minimize the smoothing effects of other kernels. Surface resampling was performed using FreeSurfer's mri_vol2surf.

fMRIPrep was additionally used to estimate the following 36 confounds from the preprocessed time series: six head motion parameters, three global signals (mean cerebrospinal fluid, white matter and whole-brain signals), temporal derivatives of the six head motion parameters and the three global signal estimates and quadratic terms for the motion parameters, tissue signals and their temporal derivatives[70,71]. These confound matrices were used within xcp_d 0.0.4, which is an extension of the top-performing eXtensible Connectivity Pipeline (XCP) Engine[70,71] specifically developed to mitigate motion-related artifacts and noise in resting-state fMRI data from developmental samples. With xcp_d, preprocessed functional time series on the fsLR cortical surface underwent nuisance regression using the 36 confounds listed above. Confounds were regressed using linear regression as implemented in Scikit-Learn (0.24.2).

Fluctuation amplitude quantification

To calculate fluctuation amplitude, defined as the power of low-frequency fMRI recordings, processed fsLR surface BOLD time series were first transformed from the time domain to the frequency domain, and a power spectrum was generated in the 0.01- to 0.08-Hz range. The mean square root of the power spectrum was then calculated. The mean square root represents the average amplitude (intensity) of time-varying resting-state BOLD fluctuations within this low-frequency band[32]. Of note, the fluctuation amplitude measure used here is analogous to other commonly used spectral- or variability-based BOLD measures, including the amplitude of low-frequency fluctuations and resting-state functional amplitude.

Fluctuation amplitude was quantified at the vertex level with xcp_d 0.0.4 and then parcellated with fsLR surface atlases to provide mean fluctuation amplitude within individual cortical regions. The Human Connectome Project multimodal parcellation (HCP-MMP) atlas[72] was used for all primary analyses and the Schaefer-400 atlas[73] was used for a sensitivity analysis. Parcellation was conducted in R with the ciftiTools package[74] using Connectome Workbench 1.5.0. Fluctuation amplitude was not analyzed within cortical regions that exhibited low signal-to-noise ratios in ≥25% of their assigned vertices. Low signal-to-noise ratio vertices were defined identically to our prior work[75] as vertices with an average (across-participant) BOLD signal of <670 after normalizing signal to a mode of 1,000. Twenty-four parcels located within the orbitofrontal cortex and the ventral temporal lobe were excluded from both the HCP-MMP atlas and the Schaefer-400 atlas.

MRI sample construction

The study sample used in the present work is comprised of individuals who received an MRI scan as part of the Philadelphia Neurodevelopmental Cohort. No statistical methods were used to predetermine the sample size of the Philadelphia Neurodevelopmental Cohort, as this was designed as a large, publicly available community data resource, but the sample size is similar to that reported in previous publications of youth brain development[42,48,66]. One thousand three hundred and seventy-four individuals in the Philadelphia Neurodevelopmental Cohort had T1w images, B0 field maps and identical-parameter[76] resting-state fMRI scans available and were considered for inclusion

in this study. From this original sample of $n = 1,374$, 120 individuals were excluded from the study due to medical problems that could impact brain function or incidentally encountered abnormalities of brain structure. Data from 202 additional participants were excluded due to low-quality T1w images and FreeSurfer reconstructions ($n = 23$) or high in-scanner head motion ($n = 179$). As in our prior work, high in-scanner head motion was defined as a mean relative root mean squared framewise displacement of >0.2 mm during the functional scan. Using data from the remaining sample ($n = 1,052$), we identified fluctuation amplitude outliers at the regional level based on a cutoff of ±4 s.d. from the mean. Individuals with outlier data in more than 5% of cortical regions ($n = 19$) were excluded, producing the final study sample of 1,033 individuals. Participants from this final study sample were not assigned to separate experimental groups or conditions; thus, data collection and analysis did not involve randomization or blinding.

Characterizing developmental effects

GAMs. All statistics were performed in R 4.0.2. To flexibly model linear and non-linear relationships between fluctuation amplitude and age, we implemented GAMs (semiparametric additive models) using the mgcv package in R[77]. GAMs were fit with regional fluctuation amplitude as the dependent variable, age as a smooth term and sex and in-scanner head motion as linear covariates. Models were fit separately for each parcellated cortical region using thin plate regression splines as the smooth term basis set and the restricted maximal likelihood approach for smoothing parameter selection. The GAM smooth term for age produces a spline, or a smooth function generated from a linear combination of weighted basis functions, that represents a region's developmental trajectory. To prevent overfitting of the spline, we set the maximum basis complexity (k) to 3 to limit the number of basis functions that could be used to estimate the overall model fit. A value of $k = 3$ was chosen over higher values (such as $k = 4-6$) given that this basis complexity resulted in the lowest model Akaike information criterion for many cortical regions and was found to appropriately capture developmental fits using a conservative number of splines. Statistical tests of the k-index[77], which estimate the degree of unaccounted for non-random pattern in the residuals, confirmed that this basis dimension was sufficient.

For each regional GAM, the significance of the association between fluctuation amplitude and age was assessed by an analysis of variance (ANOVA) that compared the full GAM model to a nested, reduced model with no age term. A significant result indicates that the residual deviance was significantly lower when a smooth term for age was included in the model, as assessed with the chi-squared test statistic. We corrected ANOVA P values across all region-wise GAMs using the FDR correction and set statistical significance at $P_{FDR} < 0.05$. For each regional GAM with a significant age smooth term, we furthermore identified the specific age range(s) wherein fluctuation amplitude was significantly changing by using the gratia package in R. Age windows of significant change were identified by quantifying the first derivative of the age smooth function (Δ fluctuation amplitude/Δ age) using finite differences and determining when the simultaneous 95% confidence interval of this derivative did not include 0 (ref. 78; two sided). To establish the overall magnitude and direction of the association between fluctuation amplitude and age, which we refer to throughout as a region's overall age effect, we calculated the partial R^2 between the full GAM model and the reduced model (effect magnitude) and signed the partial R^2 by the sign of the average first derivative of the smooth function (effect direction).

For each cortical region, we additionally tested the effects of participant sex and pubertal stage on fluctuation amplitude development. We first assessed whether the developmental trajectories of fluctuation amplitude differed between males and females by testing the significance of a factor–smooth interaction term added to the main GAM model (that is, an age-by-sex interaction that allowed age-dependent changes to vary by sex). To assess the potential influence of participant

rank orderings of ten cortical feature maps that exhibit systematic variation between lower-order sensorimotor cortices, multimodal cortices and higher-order heteromodal and paralimbic association cortices[4]. These maps include the functional hierarchy delineated by the principal gradient of functional connectivity[14], the evolutionary hierarchy defined by macaque-to-human cortical areal expansion[46], the anatomical hierarchy as quantified by the adult T1w/T2w ratio[45], allometric scaling calculated as local areal scaling with scaling of total brain size[80], aerobic glycolysis measures of brain metabolism[81], cerebral blood flow measures of brain perfusion[79], gene expression spatial variance indexed by the first PC of brain-expressed genes[45], a primary mode of brain function characterized by the first PC of NeuroSynth meta-analytic decodings[82], a histological gradient of cytoarchitectural similarity developed using the BigBrain atlas[83] and cortical thickness measured by structural MRI. The resulting S–A axis represents a dominant, large-scale motif of cortical organization that captures the stereotyped patterning of cortical heterogeneity from primary visual, somatosensory and motor regions (lowest ranks in the S–A axis) to transmodal frontal, temporal and parietal association regions (highest ranks in the S–A axis).

We performed the following analyses to ascertain whether the development of fluctuation amplitude is related to the S–A axis. Using Spearman's correlations, we evaluated associations between cortical regions' S–A axis ranks and both (1) their magnitude of fluctuation amplitude development (signed partial R^2) and (2) the age at which their fluctuation amplitude began significantly decreasing (first significant negative derivative). We next conducted a PCA on regional developmental trajectories. The goal of this PCA was to visualize the spatial axis that explained the greatest variance in how an in vivo measure of cortical intrinsic activity changed with age. The input to the PCA was region-wise age fits (zero-averaged smooth function estimates). The first PC generated by this PCA contained regional loadings that capture differences in maturational profiles across one low-dimensional embedding. We quantified the similarity between the first PC (loadings) and the cortex's S–A axis[4], anatomical hierarchy[45], functional hierarchy[14] and evolutionary hierarchy[46] with independent Spearman's correlations. We additionally assessed whether the correlation with the S–A axis was significantly greater in magnitude than correlations with the three aforementioned hierarchies using a statistical test for comparing two dependent, overlapping correlations that uses a back-transformed average Fisher's Z procedure; tests were executed using the cocor package in R[84] (hittner2003 test, two sided).

Finally, we implemented an age-resolved analysis to evaluate if the development of fluctuation amplitude aligned with the S–A axis throughout the entire developmental window studied. For this analysis, we computed across-region Spearman's correlations between S–A axis rank and the first derivative of the GAM age spline estimated at 200 ages between 8 and 23 years, producing 200 age-specific correlations. In other words, we quantified the relationship between a region's fluctuation amplitude rate of change and its position in the S–A axis at 200 age increments, allowing us to study changes in the extent of S–A axis alignment over the course of development. We determined a correlation coefficient point estimate and a 95% credible interval for these age-specific correlation values at all 200 age increments. To do so, we sampled from the posterior distribution of each region's fitted GAM 10,000 times, generating 10,000 simulated age smooth functions and corresponding derivatives. We then repeated the process of correlating S–A axis rank with the first derivative of the age smooth function at each of the 200 ages for all 10,000 posterior draws, generating a sampling distribution of possible correlation values at each age increment. This distribution was used to calculate the median correlation value (point estimate) and the 95% credible interval of correlation values at each age increment. In addition, the sampling distribution of age-specific S–A axis correlation values was used to identify the age at which fluctuation amplitude development maximally aligned with the S–A axis and

the youngest age at which no alignment to the axis was observed. To discover ages of maximal and null alignment, we calculated the age at which the axis correlation was largest and the first age at which the correlation equaled 0 for all 10,000 draws. For both measures, the median age across all draws and a 95% credible interval were calculated.

Sensitivity analyses. We performed a series of sensitivity analyses to confirm that the developmental effects observed were not being driven by potentially confounding factors, including in-scanner head motion, psychiatric medication use, cerebrovascular perfusion, BOLD signal intensity, global amplitude effects or the atlas used for cortical parcellation. For each sensitivity analysis, regional GAMs were refit either in a reduced sample (head motion and psychiatric medication analyses), in the full sample but with an additional model covariate (vascular and BOLD signal intensity analyses) or in the full sample with a modified dependent variable (global amplitude normalization and cortical atlas analyses). GAM-derived fluctuation amplitude trajectories were then visualized, and developmental alignment with the S–A axis was assessed.

The first sensitivity analysis was conducted with a low-motion sample to mitigate the potential confounding effect of in-scanner head motion on fluctuation amplitude. From the main study sample of 1,033 individuals, we excluded 343 individuals with a mean relative root mean squared framewise displacement of >0.075, retaining a low-motion sample of $n = 690$ (ages 8–23 years; mean age of 16.1 years; 395 female). The second sensitivity analysis was performed to ensure that psychotropic medication use, which was more frequent among older study participants, did not explain the age-related changes in fluctuation amplitude. GAMs were refit after removing all participants ($n = 140$) from the original sample of 1,033 individuals that reported current psychoactive medication use or a history of psychiatric hospitalization (remaining $n = 893$; ages 8–23 years; mean age of 15.6 years; 507 female).

The third sensitivity analysis aimed to address the fact that the hemodynamic BOLD signal has vascular contributions. Prior work has demonstrated that measures of BOLD fluctuation amplitude contain substantial physiological information not attributable to vascular properties, such as cerebrovascular reactivity, rigidity and blood flow[85]. Nonetheless, we still evaluated whether changes in vascular reactivity or cerebral perfusion with age could potentially be contributing to our developmental findings concerning fluctuation amplitude. We approached this evaluation by directly controlling for each participant's regional cerebral blood flow, a measure of local blood perfusion, in region-wise GAMs. Cerebral blood flow was estimated from ASL data collected from participants with a pseudocontinuous ASL sequence with the following acquisition parameters: repetition time of 4,000 ms, echo time of 2.9 ms, voxel resolution of 2.29 × 2.29 × 6 mm, label duration of 1,500 ms, postlabel delay of 1,250 ms and 40 paired label and control acquisition volumes. Data were processed using ASLPrep version 0.2.7 using the analysis pipeline reported in Adebimpe et al.[86]. Basic cerebral blood flow maps were generated and parcellated with the HCP-MMP atlas. Thirty-one participants included in the main study sample did not have ASL data available; thus, this vascular control analysis was performed using data from the remaining 1,002 participants (ages 8–23 years; mean age of 15.7 years; 552 female).

The fourth sensitivity analysis was undertaken to rule out the possibility that interindividual differences in regional mean BOLD signal intensity, rather than BOLD fluctuations per se, could account for our findings. In the full study sample ($n = 1,033$), region-specific GAMs were refit while adding regional mean BOLD signal (the average T2* signal from minimally preprocessed functional time series) as an additional control covariate. Regional mean BOLD signal was calculated from parcellated fsLR surface BOLD time series generated with fMRIPrep by averaging the BOLD signal intensity (T2*) in each parcellated cortical region across all volumes; this measure was calculated before regression of confounding signals.

The fifth sensitivity analysis used mean-normalized fluctuation amplitude as the dependent variable in all regional GAMs to examine the extent to which region-specific changes in fluctuation amplitude with age occurred above and beyond changes in global mean fluctuation amplitude. This sensitivity analysis was motivated by prior work that normalized local brain measures by a whole-brain mean to reduce interindividual differences in global values. It furthermore accounts for potential global differences in the scale of the BOLD signal across scans. Mean-normalized fluctuation amplitude was quantified for all participants ($n = 1,033$) by dividing an individual's fluctuation amplitude in each parcellated cortical region by the average fluctuation amplitude computed across all cortical regions. Notably, because whole-brain mean fluctuation amplitude declined across the age range studied, regional trajectories in this sensitivity analysis represent regional age-related decreases or increases relative to this global change.

The sixth and final sensitivity analysis was implemented to verify that the hierarchical sequence of fluctuation amplitude maturation would be observed when using a different atlas for cortical parcellation. As described above, vertex-wise fluctuation amplitude data in fsLR surface space were parcellated with the Schaefer-400 atlas. GAMs were fit using data from the main study sample of 1,033 individuals for each Schaefer atlas region.

Characterizing environmental effects

Neighborhood environment factor scores. We investigated associations between spontaneous BOLD fluctuation amplitude and neighborhood environment factor scores that index differences in neighborhood-level socioeconomic circumstances. The derivation of these factor scores has been previously explained in detail[47]. Briefly, geocoded information about each individual's neighborhood environment was extracted using their home address and the census-based American Community Survey. The first factor from an exploratory, two-factor factor analysis conducted on census variables by Moore et al.[47] is used in the present study. This neighborhood environment factor score had positive loadings for the percentage of residents who are married (loading = 0.85), median family income (0.82), the percentage of residents with a high school education (0.74), the percentage of residents who are employed (0.68) and median age (0.61) as well as negative loadings for the percentage of residents in poverty (−0.86), population density (−0.71) and the percentage of houses that are vacant (−0.60) and a weak loading for the percentage of residents who are female (−0.26). There was no correlation between age and neighborhood environment factor scores ($r = 0.01$).

GAMs. GAMs were used to investigate whether variability in youths' neighborhood environments was associated with variability in regional fluctuation amplitude. We first used GAMs to resolve age-independent main effects of the neighborhood environment by modeling environment factor scores as a linear independent variable. For each region in the HCP-MMP atlas, a GAM was fit with fluctuation amplitude as the dependent variable, age as a smooth term and sex, in-scanner motion and the environment factor score as linear covariates. These main effect models thus identify linear associations between factor scores and regional fluctuation amplitude across the entire developmental age range studied. The t value associated with the factor score term in each GAM represents the magnitude and direction of the regional fluctuation amplitude–neighborhood environment association. The significance of this association was assessed with an ANOVA that compared the full GAM model to a reduced model without the environment factor score term; ANOVA P values were FDR corrected across all region-wise GAMs.

The main effect GAMs described above were also used in a follow-up specificity analysis. The specificity analysis was conducted to evaluate whether the observed environmental effects were specific to the neighborhood environment or could be better accounted for by the household-level socioeconomic environment. To investigate this, parental education (one indicator of household socioeconomic position) was included as an additional linear covariate in regional GAMs. For each region, the significance (FDR corrected) of both the environment factor score term and the parental education term was assessed using ANOVAs as indicated above. Parental education was defined as the average years of education obtained by both parents (when data were available; $n = 943$) or by one parent ($n = 83$). Parental education information was not available for seven participants who were thus removed from this secondary analysis. Parental education was used as a proxy for household-level socioeconomic position, as other socioeconomic measures (for example, household income or parental occupational status) were not collected, although we note that individual socioeconomic position may be more robustly operationalized by combining multiple measures.

After assessing the specificity of effects to the neighborhood environment, we conducted two complementary analyses aimed at understanding whether the global cortical patterning of associations between fluctuation amplitude and neighborhood environment factor scores varies by age. We first examined main effect associations between the factor scores and regional fluctuation amplitude in groups of participants at different developmental stages. The study sample was divided into child (8–12 years; $n = 175$; 94 female), adolescent (13–17 years; $n = 405$; 225 female) and young-adult (18–23 years; $n = 299$; 167 female) groups, and region-wise main effect environment GAMs (as described above) were fit independently in each group. Regional environment factor score t values were then obtained for each group. This developmental stage analysis suggested that associations between the neighborhood environment and fluctuation amplitude may vary by age in some regions, producing changes in the cortical expression of environment effects. To further explore this possibility, we examined regional age-by-environment interactions, which explicitly model how associations between the neighborhood environment and regional fluctuation amplitude change continuously with age. In each region, we fit a varying coefficient GAM with fluctuation amplitude as the dependent variable; predictors included an age-by-factor score interaction term, a smooth term for age and control covariates including sex and in-scanner motion. These models use data from the entire sample and allow the linear association between environment factor scores and regional fluctuation amplitude to vary as a smooth function of age. Region-wise varying coefficient GAMs were used for two main objectives. First, we used these models to generate predicted trajectories of fluctuation amplitude development for low (10th percentile) and high (90th percentile) factor scores for every region. We then averaged trajectories for low and high factor scores independently within deciles of the S–A axis for visualization purposes. Second, we used these models to quantify age-specific environment effects in each region. Age-specific environment effects were computed as the slope of the linear association between fluctuation amplitude and environment factor scores at a given age (Δ fluctuation amplitude/Δ factor score). The organization of age-specific environment effects along the S–A axis was then examined across development (detailed further below).

Alignment with the S–A axis. To first assess whether the main effects of the environment on fluctuation amplitude were systematically related to the S–A axis, we tested for an association between neighborhood environment factor score t values and S–A axis ranks using a Spearman's correlation. Correlations between t values and S–A axis ranks were quantified for the primary analysis as well as for the follow-up specificity and developmental stage analyses. To additionally understand how the spatial correlation between regional brain–environment associations and S–A axis ranks changed across the entire developmental window studied, we conducted an age-resolved environmental effects analysis. Akin to the age-resolved development analysis, we computed across-region Spearman's correlations between S–A axis ranks and age-specific environment effects (varying coefficient model slopes) at

200 ages between 8 and 23 years. We determined a correlation coefficient point estimate (median correlation value) as well as a 95% credible interval for these age-specific correlation values from 10,000 draws from the posterior distribution of each region's fitted varying coefficient GAM. As in the development analysis, we also identified the age at which variation in environment effects was maximally captured by the S–A axis; a point estimate and a 95% credible interval for the age of maximal S–A axis correlation was calculated.

Spin-based spatial permutation testing

Cortical data often exhibit distance-dependent spatial autocorrelation that can inflate the significance of correlations between two cortical feature maps. To mitigate this issue, we assessed the significance of each Spearman's correlation that compared two whole-brain cortical feature maps with non-parametric, spin-based, spatially constrained rotation tests or 'spin tests'[87]. Spin tests compute a P value (denoted P_{spin}) by comparing the empirically observed correlation to a null distribution of correlations obtained by randomly spatially iterating (spinning) one of the two cortical feature maps. In particular, spin tests generate a null by rotating spherical projections of one feature map while maintaining its spatial covariance structure. The direction of the empirical Spearman's correlation can be positive or negative; the P value for the correlation is quantified as the number of times the spatial rotation-based correlation is greater than (for positive correlations) or less than (for negative correlations) the empirical correlation divided by the number of spatial rotations. Here, we generated a null distribution based on 10,000 spatial rotations. Spin tests were implemented using the rotate_parcellation algorithm in R (https://github.com/frantisekvasa/rotate_parcellation)[88].

Reporting summary

Further information on research design is available in the Nature Portfolio Reporting Summary linked to this article.

Data availability

The current study analyzes an existing, publicly available dataset from the Philadelphia Neurodevelopmental Cohort, available in the Database of Genotypes and Phenotypes (phs000607.v3.p2). Study analyses additionally made use of publicly available cortical atlases, including the HCP-MMP atlas (downloaded from https://github.com/PennLINC/xcp_d/blob/main/xcp_d/data/ciftiatlas/glasser_space-fsLR_den-32k_desc-atlas.dlabel.nii), the Schaefer-400 atlas (downloaded from https://github.com/PennLINC/xcp_d/blob/main/xcp_d/data/ciftiatlas/Schaefer2018_400Parcels_17Networks_order.dlabel.nii) and the S–A axis (downloaded from https://pennlinc.github.io/S-A_ArchetypalAxis/). Data derivatives from the current study, including development effect and environment effect maps, are available for download from https://doi.org/10.5281/zenodo.7606653.

Code availability

Neuroimaging data were processed with containerized software packages available on dockerhub. Resting-state fMRI data were processed with fMRIPrep 20.2.3 (https://hub.docker.com/r/nipreps/fmriprep/tags) and xcp_d 0.0.4 (https://hub.docker.com/r/pennlinc/xcp_abcd/tags). Following image processing, all subsequent analyses and statistics were conducted in R 4.0.2 (https://www.r-project.org) using original analysis code and Connectome Workbench 1.5.0 tools (https://www.humanconnectome.org/software/get-connectome-workbench). Original code, including code used to calculate regional fluctuation amplitude, fit regional GAMs, contextualize developmental and environmental effects and perform sensitivity analyses, has been deposited at Zenodo and is available at https://doi.org/10.5281/zenodo.7606653. A detailed description of the code and guide to code implementation is additionally provided at https://pennlinc.github.io/spatiotemp_dev_plasticity/.

References

66. Satterthwaite, T. D. et al. Neuroimaging of the Philadelphia Neurodevelopmental Cohort. *NeuroImage* **86**, 544–553 (2014).
67. Esteban, O. et al. fMRIPrep: a robust preprocessing pipeline for functional MRI. *Nat. Methods* **16**, 111–116 (2019).
68. Avants, B. B. et al. A reproducible evaluation of ANTs similarity metric performance in brain image registration. *NeuroImage* **54**, 2033–2044 (2011).
69. Dale, A. M., Fischl, B. & Sereno, M. I. Cortical surface-based analysis. I. Segmentation and surface reconstruction. *NeuroImage* **9**, 179–194 (1999).
70. Ciric, R. et al. Benchmarking of participant-level confound regression strategies for the control of motion artifact in studies of functional connectivity. *NeuroImage* **154**, 174–187 (2017).
71. Ciric, R. et al. Mitigating head motion artifact in functional connectivity MRI. *Nat. Protoc.* **13**, 2801–2826 (2018).
72. Glasser, M. F. et al. A multi-modal parcellation of human cerebral cortex. *Nature* **536**, 171–178 (2016).
73. Schaefer, A. et al. Local–global parcellation of the human cerebral cortex from intrinsic functional connectivity MRI. *Cereb. Cortex* **28**, 3095–3114 (2018).
74. Pham, D. D., Muschelli, J. & Mejia, A. F. ciftiTools: a package for reading, writing, visualizing, and manipulating CIFTI files in R. *NeuroImage* **250**, 118877 (2022).
75. Cui, Z. et al. Individual variation in functional topography of association networks in Youth. *Neuron* **106**, 340–353 (2020).
76. Covitz, S. et al. Curation of BIDS (CuBIDS): a workflow and software package for streamlining reproducible curation of large BIDS datasets. *NeuroImage* **263**, 119609 (2022).
77. Wood, S. N. *Generalized Additive Models: An Introduction with R* (Chapman and Hall/CRC, 2017).
78. Simpson, G. L. Modelling palaeoecological time series using generalised additive models. *Front. Ecol. Evol.* **6**, 149 (2018).
79. Satterthwaite, T. D. et al. Impact of puberty on the evolution of cerebral perfusion during adolescence. *Proc. Natl Acad. Sci. USA* **111**, 8643–8648 (2014).
80. Reardon, P. K. et al. Normative brain size variation and brain shape diversity in humans. *Science* **360**, 1222–1227 (2018).
81. Vaishnavi, S. N. et al. Regional aerobic glycolysis in the human brain. *Proc. Natl Acad. Sci. USA* **107**, 17757–17762 (2010).
82. Yarkoni, T., Poldrack, R. A., Nichols, T. E., Van Essen, D. C. & Wager, T. D. Large-scale automated synthesis of human functional neuroimaging data. *Nat. Methods* **8**, 665–670 (2011).
83. Paquola, C. et al. The BigBrainWarp toolbox for integration of BigBrain 3D histology with multimodal neuroimaging. *eLife* **10**, e70119 (2021).
84. Diedenhofen, B. & Musch, J. cocor: a comprehensive solution for the statistical comparison of correlations. *PLoS ONE* **10**, e0121945 (2015).
85. Garrett, D. D., Lindenberger, U., Hoge, R. D. & Gauthier, C. J. Age differences in brain signal variability are robust to multiple vascular controls. *Sci. Rep.* **7**, 10149 (2017).
86. Adebimpe, A. et al. ASLPrep: a platform for processing of arterial spin labeled MRI and quantification of regional brain perfusion. *Nat. Methods* **19**, 683–686 (2022).
87. Alexander-Bloch, A. F. et al. On testing for spatial correspondence between maps of human brain structure and function. *NeuroImage* **178**, 540–551 (2018).
88. Váša, F. et al. Adolescent tuning of association cortex in human structural brain networks. *Cereb. Cortex* **28**, 281–294 (2018).

Author contributions

V.J.S. conceived the neurodevelopmental framework and designed the study with B.L. and T.D.S. R.E.G., R.C.G. and T.D.S. provided resources and supervised collection of the neuroimaging data. D.R.R. and T.D.S. curated and quality checked the neuroimaging data. V.J.S., A.A., M.A.B., M.C. and S.C. processed the neuroimaging data with software tools developed by A.A., M.C. and S.C. V.J.S. implemented all statistical analyses with R code written by V.J.S. and B.L. A.F.A.-B. and R.T.S. provided input on statistical approaches. D.S.B. and Y.F. provided input on image analytic approaches. B.L. conducted an internal code review and technical replication of all study findings. J.S. provided data used to derive the S–A axis. T.M.M. generated the neighborhood environment factor scores, and A.P.M. provided expert guidance on environmental analyses. V.J.S. generated all figures. V.J.S. wrote the original draft and all authors (V.J.S., B.L., J.S., A.A., A.F.A.-B., D.S.B., M.A.B., M.C., S.C., Y.F., R.E.G., R.C.G., A.P.M., T.M.M., D.R.R., R.T.S. and T.D.S.) reviewed and revised the final draft.

Competing interests

The authors declare the following competing interest: R.T.S. receives consulting income from Octave Bioscience for work wholly unrelated to the present research. All other authors declare no competing interests.

Additional information

Supplementary information The online version contains supplementary material available at https://doi.org/10.1038/s41593-023-01282-y.

Correspondence and requests for materials should be addressed to Theodore D. Satterthwaite.

Peer review information *Nature Neuroscience* thanks Natalie Brito, Lucina Uddin, and the other, anonymous, reviewer(s) for their contribution to the peer review of this work.

Reprints and permissions information is available at www.nature.com/reprints.

Corresponding author(s):   Theodore D. Satterthwaite, M.D.

Last updated by author(s):   02/01/2023

Reporting Summary

Nature Portfolio wishes to improve the reproducibility of the work that we publish. This form provides structure for consistency and transparency in reporting. For further information on Nature Portfolio policies, see our Editorial Policies and the Editorial Policy Checklist.

Statistics

For all statistical analyses, confirm that the following items are present in the figure legend, table legend, main text, or Methods section.

n/a	Confirmed	
☐	☒	The exact sample size (n) for each experimental group/condition, given as a discrete number and unit of measurement
☐	☒	A statement on whether measurements were taken from distinct samples or whether the same sample was measured repeatedly
☐	☒	The statistical test(s) used AND whether they are one- or two-sided *Only common tests should be described solely by name; describe more complex techniques in the Methods section.*
☐	☒	A description of all covariates tested
☐	☒	A description of any assumptions or corrections, such as tests of normality and adjustment for multiple comparisons
☐	☒	A full description of the statistical parameters including central tendency (e.g. means) or other basic estimates (e.g. regression coefficient) AND variation (e.g. standard deviation) or associated estimates of uncertainty (e.g. confidence intervals)
☐	☒	For null hypothesis testing, the test statistic (e.g. F, t, r) with confidence intervals, effect sizes, degrees of freedom and P value noted *Give P values as exact values whenever suitable.*
☒	☐	For Bayesian analysis, information on the choice of priors and Markov chain Monte Carlo settings
☒	☐	For hierarchical and complex designs, identification of the appropriate level for tests and full reporting of outcomes
☐	☒	Estimates of effect sizes (e.g. Cohen's d, Pearson's r), indicating how they were calculated

Our web collection on statistics for biologists contains articles on many of the points above.

Software and code

Policy information about availability of computer code

Data collection	All MRI scans were acquired on a single 3 Tesla Siemens TIM Trio whole-body scanner using the VB17 revision of the Siemens software.
Data analysis	Neuroimaging data were processed with containerized software packages available on dockerhub. Resting-state functional MRI data were processed with fMRIPrep 20.2.3 (https://hub.docker.com/r/nipreps/fmriprep/tags) and xcp_d 0.0.4 (https://hub.docker.com/r/pennlinc/xcp_abcd/tags). Internal operations of fMRIPrep 20.2.3 use the following software: Advanced Normalization Tools 2.3.3, Nipype 1.6.1, FSL 5.0.9, FreeSurfer 6.0.1, AFNI 20160207. Internal operations of xcp_d 0.0.4 use the following software: Scikit-Learn 0.24.2. Following image processing, all subsequent analyses and statistics were conducted in R 4.0.2 (https://www.r-project.org) using original analysis code and Connectome Workbench 1.5.0 tools (https://www.humanconnectome.org/software/get-connectome-workbench). Original analysis code has been deposited at Zenodo and is available at https://doi.org/10.5281/zenodo.7606653. A detailed description of the original code and a guide to code implementation is additionally provided at https://pennlinc.github.io/spatiotemp_dev_plasticity.

For manuscripts utilizing custom algorithms or software that are central to the research but not yet described in published literature, software must be made available to editors and reviewers. We strongly encourage code deposition in a community repository (e.g. GitHub). See the Nature Portfolio guidelines for submitting code & software for further information.

Data

Policy information about <u>availability of data</u>

All manuscripts must include a <u>data availability statement</u>. This statement should provide the following information, where applicable:

- Accession codes, unique identifiers, or web links for publicly available datasets
- A description of any restrictions on data availability
- For clinical datasets or third party data, please ensure that the statement adheres to our <u>policy</u>

The current study analyzes an existing, publicly available dataset from the Philadelphia Neurodevelopmental Cohort, available in the Database of Genotypes and Phenotypes (phs000607.v3.p2) at https://www.ncbi.nlm.nih.gov/projects/gap/cgi-bin/study.cgi?study_id=phs000607.v3.p2. Study analyses additionally made use of publicly available cortical atlases including the HCP multimodal atlas (downloaded from https://github.com/PennLINC/xcp_d/blob/main/xcp_d/data/ciftiatlas/glasser_space-fsLR_den-32k_desc-atlas.dlabel.nii), the Schaefer-400 atlas (downloaded from https://github.com/PennLINC/xcp_d/blob/main/xcp_d/data/ciftiatlas/Schaefer2018_400Parcels_17Networks_order.dlabel.nii), and the sensorimotor-association axis (downloaded from https://pennlinc.github.io/S-A_ArchetypalAxis/). Data derivatives from the current study, including development effect and environment effect maps, are available for download from https://doi.org/10.5281/zenodo.7606653.

Human research participants

Policy information about <u>studies involving human research participants and Sex and Gender in Research.</u>

Reporting on sex and gender	This study reports on participant sex (as a biological attribute); sex was self-reported by participants. The main study sample of 1,033 individuals included 467 males and 566 females (intersex was not assessed in this study). Study findings apply to male and female sexes. Sex was considered in all statistical analyses: we conducted analyses that covaried for sex as well as an interaction analysis that assessed whether regional developmental trajectories differed between males and females. This is described in the Methods and explicitly reported in the Results.
Population characteristics	The study sample used for all primary analyses consisted of 1,033 youth (after Data Exclusions, detailed below). Study sample demographics include an age range of 8 to 23 years (mean age = 15.7 ± 3.3 years), a sex distribution of 467 males and 566 females (sex was self-reported; intersex was not assessed), and a race and ethnicity distribution (self-reported) that was 0.3% American Indian or Alaskan Native, 0.7% Asian, 41% Black or African American, 11% identifying as multiracial, and 47% White.
Recruitment	Participants in the present study were recruited as part of the Philadelphia Neurodevelopmental Cohort; participants recruited for this study had previously been assessed at the Center for Applied Genomics at the Children's Hospital of Philadelphia and the University of Pennsylvania and had provided written consent to be re-contacted for future research. The Center for Applied Genomics saw individuals referred through a pediatric health-care network of over 30 clinical community sites. Individuals were recruited into the initial Center for Applied Genomics participant pool while undergoing bloodwork, and permission was obtained to be contacted for future research recruitment. Individuals in this pool who provided consent were then re-contacted about the Philadelphia Neurodevelopmental Cohort after stratification by age, sex, and ethnicity was performed with the goal of obtaining a representative developmental sample. Individuals (ages 18-23) or their caregivers/legal guardians (ages 8-17) were first sent a letter describing the study and subsequently contacted by phone using standardized scripts. All participants were from the greater Philadelphia area. To participate in this study, individuals needed time to partake in study procedures and the ability to physically travel to the study visit. This requirement for time and travel could bias the study sample. The study sample is a community sample that includes individuals from a vast range of socioeconomic circumstances.
Ethics oversight	All study procedures were approved by the Institutional Review Boards of the University of Pennsylvania and the Children's Hospital of Philadelphia. All participants over the age of 18 gave written informed consent prior to study participation. Participants under the age of 18 gave informed assent with written parental consent. All individuals received monetary compensation for participation in the study.

Note that full information on the approval of the study protocol must also be provided in the manuscript.

Field-specific reporting

Please select the one below that is the best fit for your research. If you are not sure, read the appropriate sections before making your selection.

☒ Life sciences ☐ Behavioural & social sciences ☐ Ecological, evolutionary & environmental sciences

For a reference copy of the document with all sections, see nature.com/documents/nr-reporting-summary-flat.pdf

Life sciences study design

All studies must disclose on these points even when the disclosure is negative.

Sample size	The entire Philadelphia Neurodevelopmental Cohort is a developmental sample of 9,500 youths. From this entire sample, n = 1,601 individuals received an MRI scan and thus comprise the neuroimaging subsample of the Philadelphia Neurodevelopmental Cohort. Of the 1,601 individuals in the neuroimaging subsample, 1,374 had all neuroimaging data utilized in the present study and were thus considered for inclusion in analyses. The study therefore utilized all of the neuroimaging data made available as part of this large neurodevelopmental data resource; sample size was not chosen based on a pre-specified power analysis.
Data exclusions	As noted above, 1,374 individuals in the Philadelphia Neurodevelopmental Cohort had T1-weighted images, B0 field maps, and identical parameter resting-state functional MRI scans available. From this original sample of n = 1,374, 120 individuals were excluded from the study due to medical problems that could impact brain function or incidentally encountered abnormalities of brain structure. Data from 202 additional participants were excluded due to low quality T1-weighted images and FreeSurfer reconstructions (n = 23) or high in-scanner head motion (n = 179). As in our prior work, high in-scanner head motion was defined as a mean relative root mean squared framewise displacement > 0.2 mm during the functional scan. Using data from the remaining sample (n = 1,052), we identified fluctuation amplitude outliers at the regional level based on a cut off of ± 4 standard deviations from the mean. Individuals with outlier data in more than 5% of cortical regions (n = 19) were excluded, producing the final study sample of 1,033 individuals.
Replication	An in-depth code review and technical replication of the first author's study code was performed by the study's second author. Every analysis and result was successfully and independently reproduced internally. All code needed to reproduce experimental findings is detailed in the manuscript's code availability statement. A guide to implementing this code is additionally provided at https://pennlinc.github.io/spatiotemp_dev_plasticity.
Randomization	This study did not include separate experimental groups or conditions. Therefore, randomization was not performed.
Blinding	All study participants completed the same study protocol. Allocation into different experimental groups was not performed. Therefore, blinding was not needed.

Reporting for specific materials, systems and methods

We require information from authors about some types of materials, experimental systems and methods used in many studies. Here, indicate whether each material, system or method listed is relevant to your study. If you are not sure if a list item applies to your research, read the appropriate section before selecting a response.

Materials & experimental systems

n/a	Involved in the study
☒	Antibodies
☒	Eukaryotic cell lines
☒	Palaeontology and archaeology
☒	Animals and other organisms
☒	Clinical data
☒	Dual use research of concern

Methods

n/a	Involved in the study
☒	ChIP-seq
☒	Flow cytometry
☐	☒ MRI-based neuroimaging

Magnetic resonance imaging

Experimental design

Design type	Resting-state functional MRI
Design specifications	Eyes-open resting-state
Behavioral performance measures	No task was performed during the resting-state functional scan.

Acquisition

Imaging type(s)	T1-weighted MRI, resting-state functional MRI, B0 field map
Field strength	3 Tesla
Sequence & imaging parameters	T1-weighted MRI: T1-weighted structural images were acquired with a magnetization-prepared rapid acquisition gradient-echo (MPRAGE) sequence with the following parameters: repetition time = 1810 ms, echo time = 3.51 ms, inversion time = 1100 ms, flip angle = 9 degrees, field of view = 180 x 240 mm, matrix = 192 x 256, slice number = 160 , voxel resolution = 0.94 x 0.94 x 1 mm

Resting-state functional MRI: Resting-state functional images were acquired with a single-shot, interleaved multi-slice gradient-echo echo planar imaging (GE-EPI) sequence with the following parameters: repetition time = 3 s, echo time = 32 ms, flip angle = 90 degrees, field of view = 192 x 192 mm, matrix = 64 x 64, slice number = 46, voxel resolution = 3 mm3, volumes = 124

B0 field map: B0 field maps were acquired to enable susceptibility distortion correction of functional images. Field maps were acquired using a dual-echo, gradient-recalled echo (GRE) sequence with the following parameters: repetition time = 1000 ms, echo time 1 = 2.69 ms, echo time 2 = 5.27 ms, flip angle = 60 degrees, field of view = 240 x 240 mm, matrix = 64 x 64, slice number = 44, voxel resolution = 3.8 x 3.8 x 4 mm

Area of acquisition	A whole-brain scan was acquired
Diffusion MRI	☐ Used ☒ Not used

Preprocessing

Preprocessing software	T1-weighted images and resting-state functional MRI BOLD timeseries were processed with fMRIPrep 20.2.3. Following fMRIPrep, confound regression was performed on BOLD timeseries using xcp_d 0.0.4.
Normalization	Each T1-weighted image was non-linearly registered to the MNI152 T1 template (volume-based spatial normalization) with ANTs. BOLD timeseries were first normalized to the MNI152 T1 template and sampled onto the fsaverage surface (each participant's cortical surface was reconstructed with FreeSurfer 6.0.1 to enable surface-based analyses). Volumetric resampling of BOLD timeseries was performed using antsApplyTransforms, configured with Lanczos interpolation to minimize the smoothing effects of other kernels. Surface resampling of BOLD timeseries was performed using FreeSurfer mri_vol2surf. Finally, to project functional timeseries onto the fsLR cortical surface for study analyses, grayordinates files containing 32k vertices per hemisphere were generated using the highest-resolution fsaverage as an intermediate standardized surface space. Surface data was not smoothed.
Normalization template	Data were normalized to the MNI152 T1 template during preprocessing. BOLD timeseries were ultimately projected onto the fsLR cortical surface (32k vertices per hemisphere) for nuisance regression and the quantification of fluctuation amplitude.
Noise and artifact removal	BOLD timeseries were first corrected for head motion (six rotation and translation parameters estimated with FSL mcflirt) and susceptibility distortions (using the B0 field map) in fMRIPrep. fMRIPrep was also used to estimate the following 36 confounds from the preprocessed timeseries: six head motion parameters; three region-wise global signals (mean cerebrospinal fluid, white matter, and whole brain signals); temporal derivatives of the six head motion parameters and the three global signal estimates; and quadratic terms for the motion parameters, tissue signals, and their temporal derivatives. These confound matrices were utilized within xcp_d 0.0.4, which is an extension of the top-performing eXtensible Connectivity Pipeline (XCP) Engine specifically developed to mitigate motion-related artifacts and noise in resting-state functional MRI data from developmental samples. With xcp_d, preprocessed functional timeseries on the fsLR cortical surface underwent nuisance regression using the 36 confounds listed above. Confounds were regressed using linear regression as implemented in Scikit-Learn 0.24.2.
Volume censoring	Volumes were not censored.

Statistical modeling & inference

| Model type and settings | Developmental analyses: A generalized additive model (GAM) was fit in each cortical region. GAMs were fit with regional fluctuation amplitude as the dependent variable, age as a smooth term, and sex and in-scanner motion as linear covariates. Models were fit separately for each parcellated cortical region using thin plate regression splines as the smooth term basis set and the restricted maximal likelihood approach for smoothing parameter selection.

Environment analyses: Two classes of models were fit to explore associations between neighborhood environment factor scores and regional fluctuation amplitude. 1) Main effect models: A GAM was fit in each cortical region. Development GAMs (described above) were refit with neighborhood environment factor scores included as a linear covariate (main effect). In a follow-up specificity analysis, parental education was additionally included as a linear covariate. 2) Varying coefficient interaction models: A varying coefficient GAM was fit in each cortical region. GAMs were fit with fluctuation amplitude as the dependent variable; predictors included an age-by-factor score interaction term, a smooth term for age, and control covariates including sex and in-scanner motion. |
|---|---|
| Effect(s) tested | Developmental analyses: In each cortical region, the significance of the GAM smooth term for age was assessed through an analysis of variance (ANOVA) that compared the full GAM model to a nested, reduced model with no age term. To index the overall magnitude and direction of the age effect in each region (modeled by a spline), we calculated the partial R^2 between the full GAM model and the reduced model (effect magnitude) and signed the partial R^2 by the sign of the average first derivative of the spline (effect direction). Development model-derived statistics were correlated with myelin development data and the sensorimotor-association axis.

Environment analyses: In each cortical region, the significance of the GAM term for the neighborhood environment factor score (and parental education in the specificity analysis) was assessed by an ANOVA that compared the full GAM model to a reduced model without the environment factor score term (or the parental education term). To determine the overall magnitude and direction of the main environment effect in each region (modeled as a linear covariate), the t-value of the GAM term was used. Age-specific environment effects were also quantified from varying coefficient interaction models. Main effects of the environment and age-specific environment effects were correlated with the sensorimotor-association axis. |

Specify type of analysis:	☐ Whole brain ☐ ROI-based ☒ Both

	Anatomical location(s)	Cortical ROIs were delineated in surface space using the HCP multimodal atlas surface parcellation and the Schaefer-400 atlas surface parcellation. Cortical ROIs with low signal-to-noise ratio were excluded from analyses (N = 24 ROIs excluded from each atlas). All other cortical ROIs were included in all analyses; statistical models were run per ROI.
Statistic type for inference (See Eklund et al. 2016)		Analyses were conducted on a region-wise basis across the cortical surface.
Correction		False discovery rate (FDR) correction was applied when statistical tests were conducted across all cortical regions.

Models & analysis

n/a	Involved in the study
☒ ☐	Functional and/or effective connectivity
☒ ☐	Graph analysis
☒ ☐	Multivariate modeling or predictive analysis